

Supplementary Information

A Mechanism for Robust Circadian Timekeeping

Jae Kyoung Kim¹ and Daniel B Forger^{1, 2}

1. Department of Mathematics

2. Center for Computational Medicine and Bioinformatics, University of Michigan, Ann Arbor, Michigan 48109, USA

Table of Contents

1. Description of the detailed model.....	3
2. Description and nondimensionalization of the simple model.....	9
3. Analysis showing that a balanced stoichiometry promotes oscillations.....	13
4. Analysis of the role of an additional feedback loop in balancing stoichiometry... 	23
5. Analysis of the role of an additional negative feedback loop in maintaining a fixed period.....	27
6. Supplemental References.....	29
7. Supplementary Tables	
• Supplementary Table 1. The variables used in the detailed model	34
• Supplementary Table 2. The variables of protein complexes used in the detailed model.....	36
• Supplementary Table 3. Parameters of the detailed model.....	37
• Supplementary Table 4. Activators have a longer half-life than repressors.....	40

8. Supplementary Figures

• Supplementary Figure 1. Local sensitivity analysis of the detailed model.....	41
• Supplementary Figure 2. The transcription rate control by protein sequestration of the simple model matches experimental data.....	42
• Supplementary Figure 3. 1-1 stoichiometry generates an ultrasensitive response.....	43
• Supplementary Figure 4. Controlling the activator concentration with an additional negative feedback loop maintains stoichiometry in balance.....	44
• Supplementary Figure 5. The NNF structure oscillates over the widest range of parameters.....	46
• Supplementary Figure 6. Approximation of free activator functions in the simple model.....	48
• Supplementary Figure 7. Comparison of the predictions of the new model and experimental data.....	49
• Supplementary Figure 8. Comparison of the predictions of the previous models and experimental data.....	50
9. Equations of the detailed model.....	51

Model File

• Detailed Clock Model.....	Separate File Clock_Model.nb
• Simple Clock Model.....	Separate File Sim_Clock_Model.nb

1. Description of the detailed model

Our detailed mathematical model is built on the original model by Forger and Peskin 2003, which was revised in Ko et al. 2010. Please see these two manuscripts for a more detailed description of the model. The variables of our detailed model are listed in Supplementary Tables 1 and 2. Parameters used in the model, as well as any references used to provide estimates of parameters are listed in Supplementary Table 3. A schematic of the model can be found in Figure 1.

1) The newly included mechanisms to the previous models

- (1) *Detailed modeling of additional feedback loops:* The new model includes secondary feedback loops, which regulate the transcription of genes with a RORE in their promoters, including *Bmals* (*Bmal1* and *Bmal2*) and *Npas2*. The RORE is repressed by binding of REV-ERBs (REV-ERB α and REV-ERB β) (Liu et al, 2008; Preitner et al, 2002). Binding to the RORE is modeled with the same formalism used for E-box binding in the original model. While *Bmals* and *Npas2* mRNA are produced proportional to the activity of RORE, *Clock* mRNA is assumed to be produced at a constant rate, matching experimental data (Ueda et al, 2005). After transcription, *Bmals*, *Clock* and *Npas2* mRNA are exported to the cytoplasm and then translated. BMALs can bind with CLOCK or NPAS2, which promote phosphorylation of the complex. The phosphorylated dimer can enter the nucleus, activate transcription of promoters with an E-box and is less stable than the unphosphorylated dimer (Kwon et al, 2006).
- (2) *Updated mechanisms of BMALs-CLOCK/NPAS2 repression:* Matching recent findings, we updated the mechanisms by which the repressors (PER/CRY) inhibit the activators (BMALs-CLOCK/NPAS2) (Chen et al, 2009; Dardente et al, 2007; Kondratov et al, 2006; Ye et al, 2011). CRY1, 2 bind with BMALs-CLOCK/NPAS2 and make the dimer transcriptionally inactive as in the original model. Furthermore, CRY1, 2 binding stabilize the dimer (Dardente et al, 2007; Kondratov et al, 2006; Ye et al, 2011). With

higher affinity, PER1, 2 also bind with BMALs-CLOCK/NPAS2 and interfere with the binding of the dimer with E-box (Chen et al, 2009; Ye et al, 2011).

(3) *Accounting for the heterogeneity of different genes with E-boxes:* The *Per1/2*, *Cry1/2*, and *Rev-erbs* genes have E-boxes on their promoters and their transcription occurs proportional to the activity of the E-box. Experimental studies found that the behavior of E-boxes on these genes is different. For example, when the activators (BMAL1-CLOCK) are overexpressed, expression of *Per1, 2/Cry1, 2* shows little change while that of *Rev-erbs* significantly increases (Lee et al, 2011), which implies that the activators are saturated on the E-boxes of *Per/Cry* genes, but not *Rev-erbs*. Furthermore, the time profile of *Cry2* in SCN is almost flat unlike the other mRNAs (Ueda et al, 2005). Therefore, we introduced the three different types of E-boxes for *Per1/Per2/Cry1*, *Cry2* and *Rev-erbs*.

(4) *Inclusion of the kinase GSK3 β :* The new model includes another important kinase GSK3 β for post-translational modification of the circadian clock as well as CKI ϵ/δ . GSK3 β phosphorylates PER2 and promotes its binding with CRY and nucleus translocation (Akashi et al, 2002; Iitaka et al, 2005; Lee et al, 2001; Vielhaber et al, 2000). GSK3 β also phosphorylates the REV-ERBs and stabilizes them (Yin et al, 2006). Because GSK3 β is expressed constitutively, we assume that its concentration is constant in our model (Iitaka et al, 2005). Although the GSK3 β concentration is constant, its activity shows a circadian rhythm with a peak around ZT12 matching data from SCN (Iitaka et al, 2005). For this reason, we modeled the activity of GSK3 β with a phase similar to Cry1 mRNA because the Cry1 mRNA time profile has a peak around ZT12. We allow CKI ϵ/δ and GSK3 β to enter the nucleus only when they bind with their substrates (Lee et al, 2001).

(5) *Precise description of the effect of light on the circadian clocks:* We included a previously model of the effect of light on the circadian clocks (Kronauer et al, 1999), which quantified the human circadian pacemaker response to the light successfully. In this model, the light increase on the transcription rate of Per1-2 decreases as more light is

presented. This matches experiment data (Wilsbacher et al, 2002). In addition, we include a higher increase in Per2 transcription by light than the increase in Per1 transcription also matching experimental data (Challet et al, 2003). That is, the amplitude of *per1* and *per2* gene expression are higher about 16% and 30%, respectively, under 12:12 LD cycle with 100 lux than 12:12 DD cycle. Because light is known to increase the transcription rate of Per1/2 regardless of the E-box state (Okamura et al, 1999; Reppert & Weaver, 2002), we assumed that the light effect was independent of the E-box state as occurred in the original Forger and Peskin model.

(6) *Processes not explicitly modeled:* First, we do not distinguish between BMAL1 and BMAL2, REV-ERB α and REV-ERB β , CKI ϵ and CKI δ , or CLOCK and NPAS2 because specific functional differences between these proteins or homologs have not been found. Second, we do not model the D-box, which is one of the clock-controlled elements (Ueda et al, 2005). Third, we removed the Rorc from the model because the existence of the Rorc did not change the model behavior due to its constant mRNA level (Liu et al, 2008). Fourth, we did not model the dimerization of the REV-ERBs. Finally, we did not model the phosphorylation of GSK3 β on the CRY2 and BMAL1, which affects their degradation rate because the modest change of the amount of those proteins did not affect the model's behavior (Harada et al, 2005; Sahar et al, 2010).

2) Variables and Equations of the Detailed Model

The monomer proteins considered in our model are PER1/2, CRY1/2, BMALs, CLOCK/NPAS2, REV-ERBs, CKI, and GSK3 β . Although only 10 monomers are considered in the model, they can produce many complexes depending on the state of binding, phosphorylation and subcellular locations. To describe these all complexes, 208 variables are needed (Supplementary Tables 1 and 2): 185 variables are for proteins, 12 variables are for mRNAs, 8 variables are indicator of the promoter activity, and 2 variables are for light effect and GSK3 β activity. The model variables are listed in Supplementary Tables 1 and 2. To simply describe the approximately two hundreds complexes included in our model, which can result from bindings of PER1/2, CRY1/2, BMALs-CLOCK/NPAS2, and kinase, we use the following shorthand $x[j][k][l][m][n]$

(Ko et al, 2010) (Supplementary Table 2). The variable j, k, l and n represents the binding state of PER, CRY, kinase, and phosphorylated BMALs-CLOCK/NPAS2, respectively. The variable m represents the subcellular location. For example, $x[4][0][0][0][0]$ represents phosphorylated PER2 by CKI in the cytoplasm. $x[3][1][1][1][1]$ represents the PER2-CRY1-CKI-BMALs-CLOCK/NPAS2^P complex in the nucleus, where ^P indicates phosphorylation. Some of these variables do not exist in our model due to the restrictions of the reaction. For instance, $x[0][1][1][0][0]$ does not exist, because CRY binding with CKI is not allowed if PER1 or PER2 are not bound in our model. In this case, the variable's concentration is always zero. The reactions between these variables are described by ODE systems using explicit mass kinetics as in the original model (Forger & Peskin, 2003). The model equations are provided in the last section of the supporting information: Equations of the detailed model.

3) Parameter estimation of the detailed model

While the original model used 36 parameters, the new model has the 70 parameters due to the extensions and modifications of the model (Forger & Peskin, 2003). Despite this large number of parameters (which is still less than other models: 132 in (Mirsky et al, 2009) and 73 in (Relogio et al, 2011)), we still obtain better estimates of the parameters with newly published data and time courses.

- (1) We choose 14 parameters (degradation rate of mRNAs and proteins) matching published experimental data. These parameter values were allowed to vary up to 50% from the experimentally determined values to account for experimental error and cellular heterogeneity.
- (2) PER1's phosphorylation rate is set lower than that of PER2 (Lee et al, 2001). Light induced-Per1 transcription is set lower than light induced-Per2 transcription (Challet et al, 2003).

- (3) The dissociation constant between BMALs-CLOCK and CRY is set greater than that between BMALs-CLOCK and PER (Chen et al, 2009).
- (4) The ratio between cytoplasm and nucleus volume are limited to between 1 and 3.5 (Miller et al, 1989).
- (5) The other parameters are also restricted into a biologically reasonable range (see Supplementary Table 3).

Within these restrictions, a simulated annealing method (SA, a global stochastic parameter searcher) (Gonzalez et al, 2007) was used to estimate the parameters in two steps. First, we tried to find the parameters that provides a good fit with mRNA and protein time profiles measured in mouse suprachiasmatic nuclei (SCN) (Reppert & Weaver, 2001; Ueda et al, 2005) and relative abundance of clock proteins measured in mouse liver (Lee et al, 2001) and fibroblast (Lee et al, 2009; Lee et al, 2011) (Figures 2A-C). From this estimation, multiple parameter sets were found. Among these parameter sets, we selected several parameter sets showing qualitative matching with various knockout mutation phenotypes of mice (Table 1). Then, we used these parameter sets as initial parameter sets for another round of SA to get the final parameter set, which should a good fit with knockout mutation phenotype as well as time profiles (Supplementary Table 3). Supplementary Table 3 also indicates the changes from the original model. The references providing restrictions on parameter values are also noted in the table.

4) Validation of the detailed model with experimental data

(1) *Time profile of mRNA and proteins*: As previously mentioned, we fit the model simulations with time profiles of clock mRNA and proteins in SCN to estimate the unknown parameters. We followed the same experimental procedures used to measure time profiles. The model was entrained under 12hr-12hr Light/Dark cycle with 500lux light strength for 20 days. Then, the concentrations of mRNAs were measured during the following 48 hr in darkness and measured time courses were compared with experimental data (Ueda et al, 2005) (Figure 2A). In the same way, the simulated protein time profiles are also fit with the data (Reppert & Weaver, 2001) (Figure 2B).

(2) *Relative abundance of proteins*: Relative abundance among core clock proteins were compared with liver (Lee et al, 2001) and fibroblast data (Lee et al, 2011) because SCN data has not yet been reported (Figure 2C).

(3) *Knockout mutation phenotypes*: We also tested whether our model could predict the phenotype of mutations of clock genes (Table 1). Overall, the model simulation well matches with SCN or behavioral phenotype. Homozygous and heterozygous knockouts were simulated by reducing transcription rates by 100% and 50%, respectively. To simulate the *Rev-erba*^{-/-}, we also reduced the transcription rate of the Rev-Erb β s by 50%, which represented both Rev-erba and Rev-erb β in our model. To model the *Bmal1*^{-/-}, we reduced transcriptional rate of Bmals by 95%, which accounts for the low levels of Bmal2 when compared with Bmal1 (Ko et al, 2010). For the *Clock*^{19/+}, the half of WT CLOCK proteins were mutated to be transcriptionally inactive, yet still competed with the remaining WT CLOCK proteins.

5) Simulation of the detailed model

All the simulations were done with MATHEMATICA 8.0 (Wolfram Research). Simulation programs are available from the authors upon request.

2. Description and nondimensionalization of the simple model

The simple model is generated by modifying the well-studied Goodwin model to include an activator, which can be inactivated when bound in complex with the repressor. The mRNA (M) is transcribed proportional to the % of unbound free activator $f(P, A, K_d)$, which indicates the activity of the promoter (Buchler & Cross, 2009; Buchler & Louis, 2008). Then, as in the Goodwin model, mRNA is translated to cytoplasmic protein P_c . P_c enters the nucleus (denoted P). P then represses transcription by inhibiting activator A through binding with dissociation constant K_d .

$$\begin{aligned}\frac{dM}{dt} &= \alpha_1 f(P, A, K_d) - \beta_1 M \\ \frac{dP_c}{dt} &= \alpha_2 M - \beta_2 P_c \\ \frac{dP}{dt} &= \alpha_3 P_c - \beta_3 P \\ f(P, A, K_d) &= \frac{1}{2} \left(1 - P/A - K_d/A + \sqrt{(1 - P/A - K_d/A)^2 + 4K_d/A} \right)\end{aligned}$$

1) Single Negative Feedback Loop (SNF) Model

The model has 8 parameters. We reduce the number of parameters by scaling and assuming degradation rates are the same to increase the chance of the oscillations.

In scaling all variables, we have

$$M = \hat{M}M^*, P = \hat{P}P^*, P_c = \hat{P}_cP_c^*, A = \hat{A}A^*, K_d = \hat{K}_dK_d^*, t = \hat{t}t^*$$

and the model equations are

$$\begin{aligned}
\frac{d\hat{M}M^*}{d\hat{t}^*} &= \alpha_1 f(\hat{P}P^*, \hat{A}A^*, \hat{K}_d K_d^*) - \beta_1 \hat{M}M^* \\
\frac{d\hat{P}_c P_c^*}{d\hat{t}^*} &= \alpha_2 \hat{M}M^* - \beta_2 \hat{P}_c P_c^* \\
\frac{d\hat{P}P^*}{d\hat{t}^*} &= \alpha_3 \hat{P}_c P_c^* - \beta_3 \hat{P}P^* \\
f(\hat{P}P^*, \hat{A}A^*, \hat{K}_d K_d^*) &= \frac{1}{2} \left(1 - \hat{P}P^* / \hat{A}A^* - \hat{K}_d K_d^* / \hat{A}A^* + \sqrt{(1 - \hat{P}P^* / \hat{A}A^* - \hat{K}_d K_d^* / \hat{A}A^*)^2 + 4\hat{K}_d K_d^* / \hat{A}A^*} \right)
\end{aligned}$$

By selecting the scale of each variables as

$$M^* = \frac{\alpha_1}{\beta_1}, P_c^* = \frac{\alpha_1 \alpha_2}{\beta_1 \beta_2}, P^* = A^* = K_d^* = \frac{\alpha_1 \alpha_2 \alpha_3}{\beta_1 \beta_2 \beta_3}, t^* = \frac{1}{\beta_1}$$

and assuming the entire degradation rates are the same to increase the chance of oscillations (Forger, 2011) as

$$\beta_1 = \beta_2 = \beta_3$$

the system becomes

$$\begin{aligned}
\frac{d\hat{M}}{d\hat{t}} &= f(\hat{P}, \hat{A}, \hat{K}_d) - \hat{M} \\
\frac{d\hat{P}_c}{d\hat{t}} &= \hat{M} - \hat{P}_c \\
\frac{d\hat{P}}{d\hat{t}} &= \hat{P}_c - \hat{P} \\
f(\hat{P}, \hat{A}, \hat{K}_d) &= \frac{1}{2} \left(1 - \hat{P} / \hat{A} - \hat{K}_d / \hat{A} + \sqrt{(1 - \hat{P} / \hat{A} - \hat{K}_d / \hat{A})^2 + 4\hat{K}_d / \hat{A}} \right)
\end{aligned}$$

This system has now two non-dimensional parameters, dissociation constant (\hat{K}_d) and the concentration of the activator (\hat{A}). Because these two parameters are scaled by the all the original parameters, these two parameters represents combined effect of all original

parameters on the behavior of the system. Therefore, the model's behavior including the range of stoichiometry where the model becomes rhythmic (Figure 3D), the sensitivity of the stoichiometry (Figure 4B and Supplementary Figure 4A and 4B) and the robustness of the rhythms as parameters are perturbed (Figure 5A) can be understood by the effects of these two parameters.

2) The NNF and PNF models

This single negative feedback loop (SNF) model can be extended by adding additional negative or positive feedback loops controlling the production of activator.

$$\begin{aligned}\frac{dR}{dt} &= \gamma_1 f(P, A, K_d) - \delta_1 R \\ \frac{dA}{dt} &= \frac{\gamma_2}{R} - \delta_2 A\end{aligned}\quad (\text{Additional Negative Feedback Loop})$$

$$\begin{aligned}\frac{dR}{dt} &= \gamma_1 f(P, A, K_d) - \delta_1 R \\ \frac{dA}{dt} &= \gamma_2 R - \delta_2 A\end{aligned}\quad (\text{Additional Positive Feedback Loop})$$

We can also reduce the number of parameters by scaling the R and assuming the degradation rate of R and A are the same.

$$\begin{aligned}\frac{d\hat{R}}{d\hat{t}} &= f(\hat{P}, \hat{A}, \hat{K}_d) - \delta \hat{R} \\ \frac{d\hat{A}}{d\hat{t}} &= \frac{\gamma}{\hat{R}} - \delta \hat{A}\end{aligned}\quad (\text{Additional Negative Feedback Loop})$$

$$\begin{aligned}\frac{d\hat{R}}{d\hat{t}} &= f(\hat{P}, \hat{A}, \hat{K}_d) - \delta \hat{R} \\ \frac{d\hat{A}}{d\hat{t}} &= \gamma \hat{R} - \delta \hat{A}\end{aligned}\quad (\text{Additional Positive Feedback Loop})$$

Then, both the NNF (Negative-Negative Feedback Loops) model and the PNF (Positive-Negative Feedback Loops) model have three free parameters, a dissociation constant (\hat{K}_d), a transcription rate of the activator (γ) and a degradation rate of the activator (δ). The SNF model has two free parameters, dissociation constant (\hat{K}_d) and the fixed level of activator concentration (\hat{A}). Because $\delta = \delta_1 / \beta_1$, δ also represents the relative speed of the additional feedback loop.

3. Analysis showing that a balanced stoichiometry promotes oscillations

Recent studies have shown that when repressor binds to an activator to repress transcription, an ultrasensitive response (a large change in transcription rate for a small change in repressor or activator concentration) can be seen when the stoichiometry of the activator and repressor is near 1-1 (Buchler & Cross, 2009; Buchler & Louis, 2008). Many previous studies have argued that ultrasensitive responses can cause oscillations in feedback loops (Kim & Ferrell, 2007; Novak & Tyson, 2008). These results are built on a longstanding mathematical theory (Forger, 2011; Novak & Tyson, 2008; Thron, 1991). The combination of these results shows why a balanced stoichiometry leads to oscillations in transcription-translation feedback loops.

These previous studies also match our simulation results (Figure 3D). To provide further evidence for these results, we now provide detailed mathematical analysis of our simplified mathematical model (See below). Additionally, we showed that a 1-1 stoichiometry leads to the ultra-sensitivity in our detailed and simple models (Supplementary Figure 3A).

This analysis first considers the stability of the fixed point of the model. By the theory of Mallet-Paret and Smith, instability of the fixed point implies that the model will oscillate (Mallet-Paret & Smith, 1990). The “Secant Condition” proposed by Thron and several earlier authors can be used to determine whether the fixed point is unstable (Sontag, 2006; Thron, 1991). This gives a range of stoichiometry around 1-1 where oscillations can be seen. We then also use recent nonlinear analysis presented in (Forger, 2011) to show that if the fixed point is stable, that no oscillations can be seen. We then show that if the stoichiometry is far from 1-1, no oscillations can be seen.

1) Local Instability Analysis (which Implies Oscillations by the theory of Mallet-Paret and Smith) when $K_d=0$

The secant condition shows that the fixed point will be unstable if

$$\left| \frac{df}{dP} \frac{P}{f} \right| > (\sec \pi / 3)^3 = 8 \quad (1.1)$$

and as shown above, the nondimensionalized model has the following form:

$$\begin{aligned} dM / dt &= f(P, A, K_d) - M \\ dP_C / dt &= M - P_C \\ dP / dt &= P_C - P \end{aligned} \quad (1.2)$$

at the fixed point, $P / f = 1$, so (1.1) is equivalent to

$$\left| \frac{df}{dP} \right| > (\sec \pi / 3)^3 = 8 \quad (1.3)$$

Since the dissociation constant (K_d) is small when rhythms occur (Figure 3D), let us, for the moment, consider it to be zero (this assumption will be relaxed later). Then:

$$f(P, A, K_d) = \frac{1}{2} \left(1 - P/A - K_d/A + \sqrt{(1 - P/A - K_d/A)^2 + 4K_d/A} \right) = \begin{cases} 1 - P/A & P/A \leq 1 \\ 0 & \text{otherwise} \end{cases} = [1 - P/A]$$

Therefore, the secant condition implies that the system will oscillate if

$$\left| \frac{df}{dP} \right| = \frac{1}{A} > (\sec \pi / 3)^3 = 8$$

Since $1 - P/A = P$ at the fixed point, the model oscillates if

$$S = \frac{P}{A} = \frac{1}{A+1} > \frac{8}{9}$$

We also note, that if the steady state of stoichiometry is greater than 1, the transcription rate of this model is zero, which implies that the value of P at the fixed point would be zero. So the steady state of stoichiometry must be bounded from above by 1. Thus:

$$8/9 < S \leq 1$$

2) An accurate approximation for $f(P, A, K_d)$ when $K_d \neq 0$ and the stoichiometry is not 1-1

Before analyzing the stability of the simple model ($K_d \neq 0$), we find a simple approximation for $f(P, A, K_d)$. Since oscillations occur only when K_d is small ($< 10^{-4}$) (Figure 3D), let us assume that $\varepsilon = K_d / A$ is small which implies that the activators and repressors form a stable complex, which is also supported by experimental data (see above). Because we want to show that the model loses rhythms if the stoichiometry is not 1-1, we only consider the case where the stoichiometry is not 1-1. In this case, we can derive a simple approximation for f . That is, if the stoichiometry is

$$\frac{P}{A} \ll 1 - (2\sqrt{2\varepsilon^2 + \varepsilon} - 3\varepsilon) \text{ or } \frac{P}{A} \gg 1 + (2\sqrt{2\varepsilon^2 + \varepsilon} + 3\varepsilon)$$

(where the right hand side of these inequalities is very close to 1 when ε is small). These inequalities are equivalent to

$$(1 - \frac{P}{A} + \varepsilon)^2 \gg 4\varepsilon \frac{P}{A}$$

which allows the Taylor series expansion of f and a simple approximation for f .

$$\begin{aligned}
f(P, A, K_d) &= \frac{1}{2} \left(1 - P/A - K_d/A + \sqrt{(1 - P/A - K_d/A)^2 + 4K_d/A} \right) \\
&= \frac{1}{2} \left(1 - P/A - \varepsilon + \sqrt{(1 - P/A - \varepsilon)^2 + 4\varepsilon} \right) \\
&= \frac{1}{2} \left(1 - P/A - \varepsilon + \sqrt{(1 - P/A + \varepsilon)^2 + 4\varepsilon P/A} \right) \\
&\approx \frac{1}{2} \left(1 - P/A - \varepsilon + |(1 - P/A + \varepsilon)| + \frac{2\varepsilon P/A}{|(1 - P/A + \varepsilon)|} \right) \quad \text{if } (1 - P/A + \varepsilon)^2 \ll 4\varepsilon P/A \\
&= \begin{cases} 1 - \frac{P}{A} + \frac{\varepsilon P/A}{(1 - P/A + \varepsilon)} & \text{if } P/A \ll 1 - (2\sqrt{2\varepsilon^2 + \varepsilon} - 3\varepsilon) \text{ or } 1 - P/A + \varepsilon \gg 2\sqrt{2\varepsilon^2 + \varepsilon} - 2\varepsilon > 0 \\ \frac{\varepsilon(1+\varepsilon)}{(P/A - 1 - \varepsilon)} & \text{if } \frac{P}{A} \gg 1 + (2\sqrt{2\varepsilon^2 + \varepsilon} + 3\varepsilon) \text{ or } 1 - P/A + \varepsilon \ll -2\sqrt{2\varepsilon^2 + \varepsilon} - 2\varepsilon < 0 \end{cases} \\
&\approx \begin{cases} 1 - P/A & \text{if } P/A \ll 1 - (2\sqrt{2\varepsilon^2 + \varepsilon} - 3\varepsilon) \\ \varepsilon/(P/A - 1) & \text{if } P/A \gg 1 + (2\sqrt{2\varepsilon^2 + \varepsilon} + 3\varepsilon) \end{cases}
\end{aligned} \tag{1.4}$$

This approximation matches the original function well (see Supplementary Figures 6).

3) Local Instability Analysis (which Implies Oscillations) when $K_d \neq 0$

First, we find a lower bound of the steady state of stoichiometry (S) where the model oscillates. If $S = P/A \ll 1 - (2\sqrt{2\varepsilon^2 + \varepsilon} - 3\varepsilon)$, $f \approx 1 - P/A$ by (1.4). Then, the secant condition (1.3) implies

$$|df/dP| \approx 1/A > 8 \tag{1.5}$$

Since at the fixed point $1 - P/A \approx f = P$ or $P \approx A/(A+1)$, (1.5) is equivalent with

$$S \approx \frac{1}{A+1} > \frac{8}{9} \tag{1.6}$$

This provides the lower bound of S where the fixed point is unstable. Now, let us find the upper bound. If $S = \frac{P}{A} >> 1 + (2\sqrt{2\varepsilon^2 + \varepsilon} + 3\varepsilon)$, $f \approx \varepsilon / (P/A - 1)$. The secant condition (1.3) implies

$$|df/dP| \approx \varepsilon A / (P - A)^2 > 8 \quad (1.7)$$

Since at the fixed point $\varepsilon / (P/A - 1) \approx f = P$, (1.7) is equivalent with

$$|f'| \approx \frac{\varepsilon A}{(P-A)^2} \approx \frac{P}{P-A} = \frac{P/A}{P/A-1} > 8 \quad (1.8)$$

or

$$P/A > 8(P/A - 1) \quad (1.9)$$

From (1.9), we can get an upper bound on the steady state of stoichiometry where the fixed point is unstable:

$$S = \frac{P}{A} < \frac{8}{7} \quad (1.10)$$

Thus, (1.6) and (1.10) provides the approximate range of the steady state of stoichiometry where the model is locally unstable:

$$\frac{8}{9} < S < \frac{8}{7}$$

Indeed, this approximation matches with the actual stoichiometry range, which is calculated without approximation (see Supplementary Figure 3B). Since the instability of the fixed point implies the oscillation in the model by the theory of Mallet-Paret and

Smith, the model can be rhythmic when the steady state of the stoichiometry is around 1-1.

4) Global Stability Analysis

At the previous section, we showed that if $S < 8/7$, the model is locally stable. Here, we show that in this case, the model is globally stable (i.e. oscillation does not occur).

(1) Global Stability Conditions

The model becomes globally stable (oscillations cannot be seen) if the gain of $f(P, A, K_d)$ satisfies

$$\left| \frac{f - \langle f \rangle}{P(t) - pm} \right| < 8 \quad (1.11)$$

, where $\langle f \rangle$ is mean of f and pm is defined by $f(pm, A, K_d) = \langle f \rangle$ (Forger, 2011). The left hand side of the equation is the average slope of f between $(pm, \langle f \rangle)$ and $(P(t), f(P(t), A, K_d))$, and since $d^2f/dP^2 \geq 0$ (e.g. see Supplementary Figure 2A) we have:

$$\left| \frac{f - \langle f \rangle}{P(t) - pm} \right| \leq \left| \frac{1 - \langle f \rangle}{0 - pm} \right| = \left| \frac{1 - \langle f \rangle}{pm} \right|$$

Therefore,

$$\left| \frac{1 - \langle f \rangle}{pm} \right| < 8 \quad (1.12)$$

will be a sufficient condition to show the global stability of the model.

(2) *The average value of P is greater than or equal to the value of P at the fixed point*

The average value of P ($\langle P \rangle$) and the average value of $f(\langle f(P, A, K_d) \rangle)$ of our model

(1.2) satisfies $\langle f(P, A, K_d) \rangle = \langle P \rangle$ (Forger, 2011). Since $d^2 f / dP^2 \geq 0$,

$$\langle f(P, A, K_d) \rangle \geq f(\langle P \rangle, A, K_d) \quad (1.13)$$

or

$$\langle P \rangle = \langle f(P, A, K_d) \rangle = f(\langle P \rangle, A, K_d) + \delta \text{ and } \delta \geq 0$$

Since at the fixed point, $P = f(P, A, K_d)$, if $\delta = 0$, the average of P and the steady state of P are the same. If $\delta > 0$, the average of P is greater than the steady state of P or

$$\langle P \rangle \geq P \quad (1.14)$$

, where P represents the steady state of P .

(3) *Global Stability when $S < 8/9$*

Since $f(pm, A, K_d) = \langle P \rangle$ and $f(P, A, K_d) = P$ at the fixed point, (1.14) implies that

$$f(pm, A, K_d) = \langle P \rangle \geq P = f(P, A, K_d)$$

Since f is a decreasing function of P , we find

$$pm \leq P \quad (1.15)$$

Therefore,

$$\frac{pm}{A} \leq \frac{P}{A} = S < \frac{8}{9}$$

and we can use approximation (1.4). That is $\langle f \rangle = f(pm, A, K_d) \approx 1 - pm/A$ or $pm \approx A(1 - \langle f \rangle)$. Then, the global stability condition (1.12) is equivalent to

$$\left| \frac{1 - \langle f \rangle}{pm} \right| \approx \left| \frac{1 - \langle f \rangle}{A(1 - \langle f \rangle)} \right| = \frac{1}{A} < 8 \quad (1.16)$$

From (1.5) and (1.6), $S < 8/9$ implies that $1/A < 8$. Therefore, if $S < 8/9$, the model is globally stable as well as locally stable.

5) Bounds on the Average Stoichiometry ($\langle S \rangle$)

If $S < 8/9$, the model is globally stable and $S = \langle S \rangle$. As described above, when $S = 8/9$, the fixed point becomes unstable and oscillations are seen. At this point, stoichiometry is low and $f \approx 1 - P/A$. Then, the linearity of $f \approx 1 - P/A$ implies the equality of (1.13) and (1.14) or $S \approx \langle S \rangle$ when $S = 8/9$. Therefore, the model becomes rhythmic when the average stoichiometry is greater than $8/9$. This explains the lower bounds of the average stoichiometry that appear in Figure 3D.

Since $\langle P \rangle$ is greater than or equal to the steady state shown (1.13), the average stoichiometry ($\langle S \rangle$) is also greater than equal to the steady state of stoichiometry (S). Therefore, if $\langle S \rangle$ is less than $8/7$, then S is also less than $8/7$ and the model is rhythmic due to (1.10). Therefore, if $\langle S \rangle$ is between $8/9$ and $8/7$ or $\langle S \rangle$ is around 1-1, the model becomes rhythmic. This explains why a 1-1 average stoichiometry generates the rhythms in the model (Figure 3D). However, the upper bound is a sufficient condition (but not a

necessary one), so $\langle S \rangle$ is greater than equal to $8/7$ does not mean that the model necessarily loses rhythms.

The upper bound of $\langle S \rangle$ increases as K_d is decreases, which can be seen in Figure 3D. Here we explain this behavior. When the steady state stoichiometry S reaches its lower bound $8/9$, near the fixed point, $S = \langle S \rangle$ or $P = \langle P \rangle$ as shown above. This implies that steady state of P/A and pm/A are the same since $f(P) = P$ and $f(pm) = \langle P \rangle$. As the activator concentration decreases, both P/A and pm/A increase from $8/9$ to $8/7$. When $S = P/A$ reaches its upper bound $8/7$, we can expect $pm/A > 1 + (2\sqrt{2\varepsilon^2 + \varepsilon} + 3\varepsilon)$ as in the approximation of f above. Then, $\langle f \rangle \approx \varepsilon / (pm/A - 1) < \varepsilon / (2\sqrt{2\varepsilon^2 + \varepsilon} + 3\varepsilon)$ by (1.4). Since $\langle f \rangle = \langle p \rangle$,

$$\frac{\langle p \rangle}{A} < \frac{\varepsilon}{A(2\sqrt{2\varepsilon^2 + \varepsilon} + 3\varepsilon)} = \frac{1}{A(2\sqrt{2 + \varepsilon^{-1}} + 3)} \quad (1.16)$$

When $S = P/A$ reaches its upper bound $8/7$, by (1.7), $A = 7\sqrt{K_d/8}$ and $\varepsilon = \sqrt{8K_d}/7$.

Then (1.16) becomes

$$\frac{\langle p \rangle}{A} < \frac{\sqrt{8}}{7\sqrt{K_d}(2\sqrt{2 + 7/\sqrt{8/K_d}} + 3)} = \frac{\sqrt{8}}{7(2\sqrt{2K_d} + 7\sqrt{K_d/8} + 3\sqrt{K_d})} \approx \frac{2}{7\sqrt{7\sqrt{K_d/2}}} \quad (1.17)$$

(1.17) implies that the upper bound of average stoichiometry $\langle S \rangle$ will increase as K_d decreases, which is seen in Figure 3D. Furthermore, (1.17) explains why the model does not oscillate when K_d is too large. For instance, the upper bound of the average stoichiometry becomes 0.61 when $K_d = 10^{-3}$, which is less than the lower bound $8/9$. This is why the model does not oscillate when $K_d = 10^{-3}$ (Figure 3D). Moreover, the upper bound is 1.16 when $K_d = 10^{-4}$ which matches our simulations in Figure 3D. In summary, the mathematical analysis about the range of average stoichiometry implies that

- If $\langle S \rangle < 8/9$, the model is globally stable and does not oscillates.
- If $8/9 < \langle S \rangle < 8/7$, the model is locally unstable and oscillates.
- If $S = 8/7$, $\frac{\langle p \rangle}{A} < \frac{\sqrt{8}}{7(2\sqrt{2K_d} + 7\sqrt{K_d/8} + 3\sqrt{K_d})} \approx \frac{2}{7\sqrt{7\sqrt{K_d/2}}}$

This is in agreement with simulations shown in Figure 3D: 1) Oscillations are seen around a 1-1 stoichiometry; 2) the stoichiometry needs to be greater than 8/9 for oscillations; 3) as the dissociation constant decreases, oscillations are seen over a larger range of stoichiometry.

4. Analysis of the role of an additional feedback loop in balancing stoichiometry

Our simulations showed that an additional negative feedback loop improves the regulation of stoichiometric balance (Figure 4B and Supplementary Figure 4A and 4B). Here, we provide the mathematical analysis for the simulation results in Figure 4B and Supplementary Figure 4A and 4B. Because the model only oscillates when the dissociation constant is small ($<10^{-4}$) (Figure 3D), we assume that the dissociation constant is small for the simplicity of the analysis. In this case, the % of free activator equation can be simplified to

$$f(P, A, K_d) = \frac{1}{2} \left(1 - P/A - K_d/A + \sqrt{(1 - P/A - K_d/A)^2 + 4K_d/A} \right) \approx \begin{cases} 1 - P/A & P/A \leq 1 \\ 0 & \text{otherwise} \end{cases} = [1 - P/A]$$

1) Single Negative Feedback Loop (SNF)

With the approximation, the system can be simplified as

$$\begin{aligned} \frac{dM}{dt} &= \alpha_1 \left[1 - \frac{P}{A} \right] - \beta_1 M \\ \frac{dP_C}{dt} &= \alpha_2 M - \beta_2 P_C \\ \frac{dP}{dt} &= \alpha_3 P_C - \beta_3 P \end{aligned}$$

Then, the steady state of the system becomes

$$\frac{p/a}{[1-p/a]} a = \frac{\alpha_1 \alpha_2 \alpha_3}{\beta_1 \beta_2 \beta_3} \quad (2.1)$$

, where p and a are steady state of P and A in the system. Since activator is constant, A and a are the same. Then,

$$\frac{1-\varepsilon}{\varepsilon} = C/a = C_1 \quad (2.2)$$

, where $\varepsilon = [1 - p/a]$ representing the steady state of % of free activator and C_1 represents all parameters of the system.

$$\varepsilon = \frac{1}{1+C_1} \quad (2.3)$$

Now, let's calculate the relative sensitivity of ε with respect to C_1 from the above equation. If this sensitivity is low, then we can expect the % of free activator of this system is stable for the perturbation of any parameters.

$$\frac{d\varepsilon}{dC_1} \frac{C_1}{\varepsilon} = \frac{-1}{(1+C_1)^2} C_1 \frac{1+C_1}{1} = \frac{-C_1}{1+C_1} \quad (2.4)$$

Because the system oscillates only when the stoichiometry between p and a is close to 1 (Figure 3D), ε will become close to 0 and C_1 becomes large from (2.2) or (2.3) when the model oscillates. Therefore, we can expect the relative sensitivity would be around -1 from (2.4) (Supplementary Figure 4C).

2) Negative Feedback Loop with an Additional Negative Feedback Loop (NNF)

Additional secondary loop in the NNF also becomes simple with the assumption $K_d=0$.

$$\begin{aligned} \frac{dR}{dt} &= \gamma_1 \left[1 - \frac{P}{A} \right] - \delta_1 R \\ \frac{dA}{dt} &= \frac{\gamma_2}{R} - \delta_2 A \end{aligned}$$

Then, the steady state of the activator A becomes

$$a = \frac{\gamma_2 \delta_1}{\gamma_1 \delta_2} \frac{1}{[1 - p/a]} = \frac{D}{[1 - p/a]} = \frac{D}{\varepsilon} \quad (2.5)$$

By combining two steady state equations (2.1) and (2.5), we can get

$$\frac{1-\varepsilon}{\varepsilon} a = \frac{1-\varepsilon}{\varepsilon} \frac{D}{\varepsilon} = C \Leftrightarrow \frac{1-\varepsilon}{\varepsilon^2} = C/D = C_2$$

Again, C_2 represents the all parameters in NNF.

$$\begin{aligned} \varepsilon &= \frac{-1 + \sqrt{1 + 4C_2}}{2C_2} \\ \frac{d\varepsilon}{dC_2} \frac{C_2}{\varepsilon} &= \left(\frac{1}{C_2 \sqrt{1 + 4C_2}} - \frac{-1 + \sqrt{1 + 4C_2}}{2C_2^2} \right) C_2 \frac{2C_2}{-1 + \sqrt{1 + 4C_2}} \end{aligned}$$

For small ε , the relative sensitivity becomes about -0.5 (Supplementary Figure 4C), which is half of that of SNF.

3) Negative Feedback Loop with an Additional Positive Feedback Loop (PNF)

In a similar way used to analyze NNF, we can also derive the steady state of the activator in PNF,

$$a = \frac{\gamma_1 \gamma_2}{\delta_1 \delta_2} [1 - p/a] = E [1 - p/a] \quad (2.6)$$

By combining two steady state equations (2.2) and (2.6), we can get

$$\frac{1-\varepsilon}{\varepsilon} A = \frac{1-\varepsilon}{\varepsilon} E \varepsilon = C \Leftrightarrow 1-\varepsilon = C/E = C_3 \quad (7)$$

$$\varepsilon = 1 - C_3 \quad (2.8)$$

$$\frac{d\varepsilon}{dC_3} \frac{C_3}{\varepsilon} = -C_3 \frac{1}{1-C_3} = \frac{-C_3}{1-C_3} \quad (2.9)$$

For small ε , $1 - C_3$ is small by (2.8). Then, we can expect the sensitivity will be huge for small ε (Supplementary Figure 4C) from (2.9). In fact, by combining (2.8) and (2.9),

$$\frac{d\varepsilon}{dC_3} \frac{C_3}{\varepsilon} = \frac{-C_3}{1-C_3} = \frac{-1+\varepsilon}{\varepsilon} \approx \frac{1}{\varepsilon}$$

We can see that the sensitivity is approximately $1/\varepsilon$.

4) Summary

The relative sensitivity of the % of free activator (ε) for any parameter perturbation becomes about 1, 0.5 and $1/\varepsilon$ in NF, NNF and PNF, respectively (Supplementary Figure 4C). This means % of free activator (ε) is most robust for parameter perturbation in NNF structure. Because $\varepsilon = [1 - p/a] = [1 - stoichiometry]$, the robustness of ε in NNF implies the robustness of stoichiometry in the NNF structure. In the previous section, we showed that the model becomes rhythmic when the steady state of stoichiometry is in appropriate range (Supplementary Figure 4C). Since an additional negative feedback loop improves the regulation of the stoichiometric balance, the NNF structure is the best to maintain the rhythms for the perturbations.

5. Analysis of the role of an additional negative feedback loop in maintaining a fixed period

We showed that the NNF structure has a nearly constant period in the presence of large changes in gene expression levels (Figure 6D). Here, we provide the mathematical analysis for the simulation results in Figure 6D. As we showed at the previous section, the simple model can be approximated as

$$\begin{aligned} dM / dt &= \lfloor 1 - P / A \rfloor - M \\ dP_C / dt &= M - P_C \\ dP / dt &= P_C - P \end{aligned} \quad (3.1)$$

If the transcription rate is increased by α , then the model is changed to

$$\begin{aligned} dM / dt &= \alpha \lfloor 1 - P / A \rfloor - M \\ dP_C / dt &= M - P_C \\ dP / dt &= P_C - P \end{aligned} \quad (3.2)$$

If we define new variable $\tilde{M} = M / \alpha$, $\tilde{P}_C = P_C / \alpha$ and $\tilde{P} = P / \alpha$, the model (3.2) becomes

$$\begin{aligned} d\tilde{M} / dt &= \lfloor 1 - \alpha \tilde{P} / A \rfloor - \tilde{M} \\ d\tilde{P}_C / dt &= \tilde{M} - \tilde{P}_C \\ d\tilde{P} / dt &= \tilde{P}_C - \tilde{P} \end{aligned} \quad (3.3)$$

These equations are the same with the original equations (3.1) except for the transcription term, $\lfloor 1 - \alpha \tilde{P} / A \rfloor$. We have shown that the additional negative feedback loop maintains the stoichiometric balance by adjusting the level of the activators according to the change of the repressor levels. In this case, the repressor level is increased by α , so in ideal case, the activator level (A) can be increased by α through the additional negative feedback

loop. This makes $\lfloor 1 - \alpha \tilde{P} / A \rfloor$ to the $\lfloor 1 - \tilde{P} / A \rfloor$. That is, with the additional negative feedback loop, (3.3) becomes

$$\begin{aligned} d\tilde{M} / dt &= \lfloor 1 - \tilde{P} / A \rfloor - \tilde{M} \\ d\tilde{P}_C / dt &= \tilde{M} - \tilde{P}_C \\ d\tilde{P} / dt &= \tilde{P}_C - \tilde{P} \end{aligned} \quad (3.4)$$

Therefore, the model (3.4) has the solution with the same period of the solution of the original model (3.1) while the amplitude of solution (\tilde{P}) is increased by α since $\tilde{P} = P / \alpha$.

6. Supporting References

- Akashi M, Tsuchiya Y, Yoshino T, Nishida E (2002) Control of intracellular dynamics of mammalian period proteins by casein kinase I epsilon (CKIepsilon) and CKIdelta in cultured cells. *Mol Cell Biol* **22**: 1693-1703
- Baggs JE, Price TS, DiTacchio L, Panda S, Fitzgerald GA, Hogenesch JB (2009) Network features of the mammalian circadian clock. *PLoS Biol* **7**: e52
- Becker-Weimann S, Wolf J, Herzl H, Kramer A (2004) Modeling feedback loops of the Mammalian circadian oscillator. *Biophys J* **87**: 3023-3034
- Buchler NE, Cross FR (2009) Protein sequestration generates a flexible ultrasensitive response in a genetic network. *Mol Syst Biol* **5**: 272
- Buchler NE, Louis M (2008) Molecular titration and ultrasensitivity in regulatory networks. *J Mol Biol* **384**: 1106-1119
- Busino L, Bassermann F, Maiolica A, Lee C, Nolan PM, Godinho SI, Draetta GF, Pagano M (2007) SCFFbxl3 controls the oscillation of the circadian clock by directing the degradation of cryptochrome proteins. *Science* **316**: 900-904
- Challet E, Poirel VJ, Malan A, Pevet P (2003) Light exposure during daytime modulates expression of Per1 and Per2 clock genes in the suprachiasmatic nuclei of mice. *J Neurosci Res* **72**: 629-637
- Chawla A, Lazar MA (1993) Induction of Rev-ErbA alpha, an orphan receptor encoded on the opposite strand of the alpha-thyroid hormone receptor gene, during adipocyte differentiation. *J Biol Chem* **268**: 16265-16269
- Chen R, Schirmer A, Lee Y, Lee H, Kumar V, Yoo SH, Takahashi JS, Lee C (2009) Rhythmic PER abundance defines a critical nodal point for negative feedback within the circadian clock mechanism. *Mol Cell* **36**: 417-430
- Dardente H, Fortier EE, Martineau V, Cermakian N (2007) Cryptochromes impair phosphorylation of transcriptional activators in the clock: a general mechanism for circadian repression. *Biochem J* **402**: 525-536
- Forger DB (2011) Signal processing in cellular clocks. *Proc Natl Acad Sci U S A* **108**: 4281-4285
- Forger DB, Peskin CS (2003) A detailed predictive model of the mammalian circadian clock. *Proc Natl Acad Sci U S A* **100**: 14806-14811

Froy O, Chang DC, Reppert SM (2002) Redox potential: differential roles in dCRY and mCRY1 functions. *Curr Biol* **12**: 147-152

Gonzalez OR, Kuper C, Jung K, Naval PC, Jr., Mendoza E (2007) Parameter estimation using Simulated Annealing for S-system models of biochemical networks. *Bioinformatics* **23**: 480-486

Griffith JS (1968) Mathematics of cellular control processes. I. Negative feedback to one gene. *J Theor Biol* **20**: 202-208

Harada Y, Sakai M, Kurabayashi N, Hirota T, Fukada Y (2005) Ser-557-phosphorylated mCRY2 is degraded upon synergistic phosphorylation by glycogen synthase kinase-3 beta. *J Biol Chem* **280**: 31714-31721

Iitaka C, Miyazaki K, Akaike T, Ishida N (2005) A role for glycogen synthase kinase-3beta in the mammalian circadian clock. *J Biol Chem* **280**: 29397-29402

Kim SY, Ferrell JE, Jr. (2007) Substrate competition as a source of ultrasensitivity in the inactivation of Wee1. *Cell* **128**: 1133-1145

Ko CH, Yamada YR, Welsh DK, Buhr ED, Liu AC, Zhang EE, Ralph MR, Kay SA, Forger DB, Takahashi JS (2010) Emergence of noise-induced oscillations in the central circadian pacemaker. *PLoS Biol* **8**: e1000513

Kondratov RV, Kondratova AA, Lee C, Gorbacheva VY, Chernov MV, Antoch MP (2006) Post-translational regulation of circadian transcriptional CLOCK(NPAS2)/BMAL1 complex by CRYPTOCHROMES. *Cell Cycle* **5**: 890-895

Kronauer RE, Forger DB, Jewett ME (1999) Quantifying human circadian pacemaker response to brief, extended, and repeated light stimuli over the phototopic range. *J Biol Rhythms* **14**: 500-515

Kwon I, Lee J, Chang SH, Jung NC, Lee BJ, Son GH, Kim K, Lee KH (2006) BMAL1 shuttling controls transactivation and degradation of the CLOCK/BMAL1 heterodimer. *Mol Cell Biol* **26**: 7318-7330

Lamaze A, Lamouroux A, Vias C, Hung HC, Weber F, Rouyer F (2011) The E3 ubiquitin ligase CTRIP controls CLOCK levels and PERIOD oscillations in Drosophila. *EMBO Rep* **12**: 549-557

Lee C, Etchegaray JP, Cagampang FR, Loudon AS, Reppert SM (2001) Posttranslational mechanisms regulate the mammalian circadian clock. *Cell* **107**: 855-867

Lee H, Chen R, Lee Y, Yoo S, Lee C (2009) Essential roles of CKIdelta and CKIepsilon in the mammalian circadian clock. *Proc Natl Acad Sci U S A* **106**: 21359-21364

Lee Y, Chen R, Lee HM, Lee C (2011) Stoichiometric relationship among clock proteins determines robustness of circadian rhythms. *J Biol Chem* **286**: 7033-7042

Leloup JC, Goldbeter A (2004) Modeling the mammalian circadian clock: sensitivity analysis and multiplicity of oscillatory mechanisms. *J Theor Biol* **230**: 541-562

Liu AC, Tran HG, Zhang EE, Priest AA, Welsh DK, Kay SA (2008) Redundant function of REV-ERB α and beta and non-essential role for Bmal1 cycling in transcriptional regulation of intracellular circadian rhythms. *PLoS Genet* **4**: e1000023

Mallet-Paret J, Smith H (1990) The Poincare-Bendixon theorem for monotone cyclic feedback systems. *Journal of Dynamics and Differential Equations* **2**: 367-421

Meng QJ, Logunova L, Maywood ES, Gallego M, Lebiecki J, Brown TM, Sladek M, Semikhodskii AS, Glossop NR, Piggins HD, Chesham JE, Bechtold DA, Yoo SH, Takahashi JS, Virshup DM, Boot-Hanford RP, Hastings MH, Loudon AS (2008) Setting clock speed in mammals: the CK1 epsilon tau mutation in mice accelerates circadian pacemakers by selectively destabilizing PERIOD proteins. *Neuron* **58**: 78-88

Miller MM, Gould BE, Nelson JF (1989) Aging and long-term ovariectomy alter the cytoarchitecture of the hypothalamic-preoptic area of the C57BL/6J mouse. *Neurobiol Aging* **10**: 683-690

Mirsky HP, Liu AC, Welsh DK, Kay SA, Doyle FJ, 3rd (2009) A model of the cell-autonomous mammalian circadian clock. *Proc Natl Acad Sci U S A* **106**: 11107-11112

Novak B, Tyson JJ (2008) Design principles of biochemical oscillators. *Nat Rev Mol Cell Biol* **9**: 981-991

Okamura H, Miyake S, Sumi Y, Yamaguchi S, Yasui A, Muijtjens M, Hoeijmakers JH, van der Horst GT (1999) Photic induction of mPer1 and mPer2 in cry-deficient mice lacking a biological clock. *Science* **286**: 2531-2534

Preitner N, Damiola F, Lopez-Molina L, Zakany J, Duboule D, Albrecht U, Schibler U (2002) The orphan nuclear receptor REV-ERB α controls circadian transcription within the positive limb of the mammalian circadian oscillator. *Cell* **110**: 251-260

Relogio A, Westermark PO, Wallach T, Schellenberg K, Kramer A, Herzog H (2011) Tuning the mammalian circadian clock: robust synergy of two loops. *PLoS Computational Biology* **7**: e1002309

Relógio A, Westermark PO, Wallach T, Schellenberg K, Kramer A, Herzog H (2011) Tuning the Mammalian Circadian Clock: Robust Synergy of Two Loops. *PLoS Computational Biology* **7**: e1002309

Reppert SM, Weaver DR (2001) Molecular analysis of mammalian circadian rhythms. *Annu Rev Physiol* **63**: 647-676

Reppert SM, Weaver DR (2002) Coordination of circadian timing in mammals. *Nature* **418**: 935-941

Sahar S, Zocchi L, Kinoshita C, Borrelli E, Sassone-Corsi P (2010) Regulation of BMAL1 protein stability and circadian function by GSK3beta-mediated phosphorylation. *PLoS One* **5**: e8561

Siepka SM, Yoo SH, Park J, Song W, Kumar V, Hu Y, Lee C, Takahashi JS (2007) Circadian mutant Overtime reveals F-box protein FBXL3 regulation of cryptochrome and period gene expression. *Cell* **129**: 1011-1023

Sontag ED (2006) Passivity gains and the “secant condition” for stability. *Systems & Control Letters* **55**: 177-183

Suter DM, Molina N, Gatfield D, Schneider K, Schibler U, Naef F (2011) Mammalian genes are transcribed with widely different bursting kinetics. *Science* **332**: 472-474

Syed S, Saez L, Young MW (2011) Kinetics of doubletime kinase-dependent degradation of the Drosophila period protein. *J Biol Chem* **286**: 27654-27662

Thron CD (1991) The secant condition for instability in biochemical feedback control. I. The role of cooperativity and saturability. *Bulletin of Mathematical Biology*: 383-401

Ueda HR, Hayashi S, Chen W, Sano M, Machida M, Shigeyoshi Y, Iino M, Hashimoto S (2005) System-level identification of transcriptional circuits underlying mammalian circadian clocks. *Nat Genet* **37**: 187-192

Vielhaber E, Eide E, Rivers A, Gao ZH, Virshup DM (2000) Nuclear entry of the circadian regulator mPER1 is controlled by mammalian casein kinase I epsilon. *Mol Cell Biol* **20**: 4888-4899

Wilsbacher LD, Yamazaki S, Herzog ED, Song EJ, Radcliffe LA, Abe M, Block G, Spitznagel E, Menaker M, Takahashi JS (2002) Photic and circadian expression of luciferase in mPeriod1-luc transgenic mice invivo. *Proc Natl Acad Sci U S A* **99**: 489-494

Ye R, Selby CP, Ozturk N, Annayev Y, Sancar A (2011) Biochemical analysis of the canonical model for the mammalian circadian clock. *J Biol Chem* **286**: 25891-25902

Yin L, Wang J, Klein PS, Lazar MA (2006) Nuclear receptor Rev-erbalpha is a critical lithium-sensitive component of the circadian clock. *Science* **311**: 1002-1005

7. Supplementary Tables

Supplementary Table 1. The variables used in the detailed model.

Name	Symbol
The concentration of <i>Per1</i> mRNA in the nucleus/ cytoplasm	MnPo/McPo
The concentration of <i>Per2</i> mRNA in the nucleus/ cytoplasm	MnPt/McPt
The concentration of <i>Cry1</i> mRNA in the nucleus/ cytoplasm	MnRo/McRo
The concentration of <i>Cry2</i> mRNA in the nucleus/ cytoplasm	MnRt/McRt
The concentration of <i>Bmals</i> mRNA in the nucleus/ cytoplasm	MnB/McB
The concentration of <i>Npas2</i> mRNA in the nucleus/ cytoplasm	MnNp/McNp
The concentration of <i>Rev-erbs</i> mRNA in the nucleus/cytoplasm	MnRev/McRev
The concentration of BMALs protein in the cytoplasm	B
The concentration of CLOCK/NPAS2 protein in the cytoplasm	Cl
The concentration of unphosphorylated BMALs-CLOCK/NPAS2	BC
The concentration of unphosphorylated REV-ERBs in the nucleus/cytoplasm	revn/cyrev
The concentration of unphosphorylated REV-ERBs bound with GSK3 β in the nucleus/cytoplasm	revng/cyrevg
The concentration of phosphorylated REV-ERBs bound with GSK3 β in the nucleus/cytoplasm	revngp/cyrevgp
The concentration of phosphorylated REV-ERBs in the nucleus/cytoplasm	revnp/cyrevp
The probability of the <i>per1</i> , <i>per2</i> , and <i>cry1</i> E-box being activated	G
The probability of the <i>per1</i> , <i>per2</i> , and <i>cry1</i> E-box being repressed	GR
The probability of the <i>cry2</i> E-box being activated	Gc
The probability of the <i>cry2</i> E-box being repressed	GcR
The probability of the <i>rev-erbs</i> E-box being activated	Gr
The probability of the <i>rev-erbs</i> E-box being repressed	GrR
The probability of the <i>npas2</i> and <i>cry1</i> RORE being activated	GB
The probability of the <i>npas2</i> and <i>cry1</i> RORE being repressed	GBR

The probability of the <i>Bmals</i> RORE being activated	GBb
The probability of the <i>Bmals</i> RORE being repressed	GBRb
The activity of GSK3 β	gto
The strength of transcription drive of light	ltn

Note the protein complexes are separately listed in Supplementary Table 2.

Supplementary Table 2. The variables of protein complexes used in our detailed model.

	j	k	l	m	n
Index	PER	CRY	Kinase	Location	BMALs-CLK
0	No PER bound	No CRY bound	No Kinases bound	Cytoplasm	No BMALs-CLK bound
1	PER1	CRY1	CKI	Nucleus	BMALs ^P -CLK ^P
2	PER1 ^P by CKI	CRY2	GSK3		
3	PER2		CKI&GSK3		
4	PER2 ^P by CKI				
5	PER2 ^P by GSK3				
6	PER2 ^P by both GSK3 and CKI				

Each complex is encoded as $x[j][k][l][m][n]$, where j, k, l, m and n refer to the proteins that are present in the complex, or the location of the complex. We also assume that when BMALs-CLK is phosphorylated when in complex. “^P” represents “phosphorylated”. Further details can be seen in the section “Equations of the Detailed Model.”

Supplementary Table 3. Parameters of the Detailed Model.

Parameter Description	Symbol	Value	Reference
Transcription rate constant for <i>Per1</i>	trPo	25.92	
Transcription rate constant for <i>Per2</i>	trPt	44.85	
Transcription rate constant for <i>Cry1</i>	trRo	23.07	
Transcription rate constant for <i>Cry2</i>	trRt	39.94	
Transcription rate constant for <i>Bmal</i> (1)	trB	46.10	
Transcription rate constant for <i>Npas2</i> (1)	trNp	0.33	
Transcription rate constant for <i>Rev-Erb</i> s	trRev	102.9	
Translation rate constant for PER1 and PER2	tlp	1.81	
Translation rate constant for CRY1 and CRY2	tlr	5.038	
Translation rate constant for BMAL (1)	tlb	0.53	
Translation rate constant for CLOCK (1)	tlc	4.645	
Translation rate constant for NPAS2 (1)	tlnp	1.251	
Translation rate constant for REV-ERBs	tlrev	8.907	
Binding rate constant for PER2 to GSK3 β (4)	agp	1.396	
Binding rate constant for REV-ERBs to GSK3 β (4)	ag	0.162	
Unbinding rate constant for PER2/REV-ERBs to GSK3 β (4)	dg	2.935	
Binding rate constant for PER1/2 to CKI ϵ/δ	ac	0.046	
Unbinding rate constant for PER1/2 to CKI ϵ/δ	dc	0.108	
Binding rate constant for PER1/2 to CRY1/2	ar	0.024	
Unbinding rate constant for PER1/2 to CRY1/2	dr	0.605	
Binding rate constant for PER1/2 to BMAL-CLOCK/NPAS2 in the nucleus (2)	bbin	6.926	(Chen et al, 2009)
Unbinding rate constant for PER1/2 to BMAL-CLOCK/NPAS2 in the nucleus (2)	unbbin	0.13	(Chen et al, 2009)
Binding rate constant for CRY1/2 to BMAL-CLOCK/NPAS2 in the nucleus (2)	cbbin	6.599	(Chen et al, 2009)
Unbinding rate constant for CRY1/2 to BMAL-CLOCK/NPAS2 in the nucleus (2)	uncbbin	0.304	(Chen et al, 2009)
Binding rate constant for BMAL to CLOCK/NPAS2 (1)	cbin	0.045	
Unbinding rate constant for BMAL to CLOCK/NPAS2 (1)	uncbin	7.272	
Binding rate constant for REV-ERBs to GSK3 β (4)	ag	0.162	
Normalized binding rate constant for BMAL-CLOCK/NPAS2 to <i>Per1/2/Cry1</i> E-box (3)	bin	6.972	
Normalized unbinding rate constant for BMAL-CLOCK/NPAS2 to <i>Per1/2/Cry1</i> E-box (3)	unbin	0.255	
Normalized binding rate constant for BMAL-CLOCK/NPAS2 to <i>Cry2</i> E-box (3)	binc	0.280	
Normalized unbinding rate constant for BMAL-CLOCK/NPAS2 to <i>Cry2</i> E-box (3)	unbinc	0.009	
Normalized binding rate constant for BMAL-CLOCK/NPAS2 to <i>Rev-erb</i> s E-box (3)	binr	6.154	
Normalized unbinding rate constant for BMAL-CLOCK/NPAS2 to <i>Rev-erb</i> s E-box (3)	unbinr	2.91	
Normalized binding rate constant for REV-ERBs to <i>Bmal</i> RORE (1)	binrevb	0.006	

Normalized unbinding rate constant for REV-ERBs to <i>Bmal</i> RORE (1)	unbinre vb	5.305	
Normalized binding rate constant for REV-ERBs to <i>Cry1/Npas2</i> RORE (1)	binrev	0.012	
Normalized unbinding rate constant for REV-ERBs to <i>Cry1/Npas2</i> RORE (1)	unbinre v	10.97	
Rate constant for folding and nuclear export of <i>Per1/2</i> , <i>Cry1/2</i> , <i>Bmal</i> and <i>Npas2</i> mRNA	tmc	0.164	
Rate constant for folding and nuclear export of <i>Rev-Erb</i> s mRNA	tmcrev	9.263	
Nuclear localization rate constant for proteins bound to PER	nl	0.643	
Nuclear export rate constant for protein bound to PER	ne	0.026	
Nuclear localization rate constant for REV-ERBs as well as GSK3 β if bound (4)	nlrev	9.637	
Nuclear export rate constant for REV-ERBs as well as GSK3 β if bound (4)	nerve	0.015	
Nuclear localization rate constant for BMAL-CLOCK/NPAS2 (1)	nlbc	5.265	
Nuclear export rate constant for unbound kinases GSK3 β and CKI (4)	lne	0.595	
Total CK1 concentration	Ct	57.61	(Lee et al, 2001)
Total GSK3 β concentration (4)	Gt	79.73	
CKI ϵ/δ phosphorylation rate constant for PER1	hoo	0.527	(Lee et al, 2001)
CKI ϵ/δ phosphorylation rate constant for PER2	hto	2.456	(Lee et al, 2001)
Phosphorylation rate constant for BMAL-CLOCK/NPAS2 (1)	phos	0.291	
Increase rate of GSK3 β activity (4)	trgto	0.644	
Decrease rate of GSK3 β activity (4)	ugto	0.063	
Degradation rate constant for <i>Per1</i>	umPo	0.765	(Siepka et al, 2007)
Degradation rate constant for <i>Per2</i>	umPt	0.589	(Siepka et al, 2007)
Degradation rate constant for <i>Cry1</i>	umRo	0.403	(Siepka et al, 2007)
Degradation rate constant for <i>Cry2</i>	umRt	0.456	(Siepka et al, 2007)
Degradation rate constant for <i>Bmal</i> (1)	umB	0.795	(Suter et al, 2011)
Degradation rate constant for <i>Npas2</i> (1)	umNp	0.369	
Degradation rate constant for <i>Rev-Erb</i> s	umRev	1.51	(Chawla & Lazar, 1993)
Degradation rate constant for unphosphorylated PER	upu	0.07	(Lee et al, 2009)
Degradation rate constant for CKI phosphorylated PER	up	3.537	(Meng et al, 2008)
Degradation rate constant for CRY1	uro	0.174	(Siepka et al, 2007)
Degradation rate constant for CRY2	urt	0.482	(Busino et al, 2007; Chen et al, 2009)
Degradation rate constant for BMAL (1)	ub	0.019	(Kwon et al, 2006)
Degradation rate constant for CLOCK/NPAS2 (1)	uc	0.025	(Kwon et al, 2006)
Degradation rate constant for BMAL-CLOCK/NPAS2 (1)	ubc	0.349	(Kwon et al, 2006)
Degradation rate constant for unphosphorylated REV-ERBs (4)	urev	1.649	(Suter et al, 2011)
Degradation rate constant for GSK3 β phosphorylated	uprev	0.517	(Suter et al, 2011)

REV-ERBs (4)			
Ratio of nuclear to cytoplasmic compartment volume	Nf	3.351	(Miller et al, 1989)
Additional <i>Per1</i> transcription rate in the presence of light(5)	lono	0.206	(Challet et al, 2003)
Additional <i>Per2</i> transcription rate in the presence of light (5)	lont	0.396	(Challet et al, 2003)
Light level (5)	ltI	500	(Kronauer et al, 1999)
Rate of activation of pho (5)	lta	0.607	(Kronauer et al, 1999)
Light effect decrease (backward) rate (5)	ltb	0.013	(Kronauer et al, 1999)

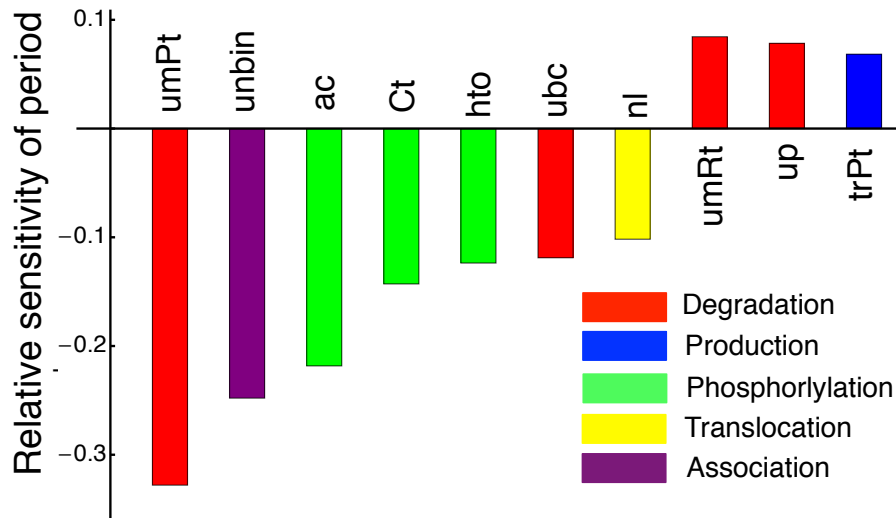
References presenting experimental data on the parameter are indicated. If a parameter has been newly added to the previous model, a number is presented after the parameter description. This number corresponds to the list that describes the changes that were made to the model in the section: A description of the detailed model. The units of time are hours, concentrations are expressed in nM and light is presented in Lux. As described in Forger and Peskin 2003, binding rates to promoter elements are considered “normalized” because they are tracked by the probability that they are unbound. Further details can be found in Forger and Peskin 2003.

Supplementary Table 4. Activators have a longer half-life than repressors.

		Mice Fibroblasts	<i>Drosophila</i> S2 cells	
Repressors	PER	PER ^P	CRY	dPER
Half-Life(hr)	13	1.4	3.1-5.2	1.5
Activators	BMAL1	CLOCK	BMAL1-CLK	dCLOCK
Half-Life(hr)	47	13	3	6

The endogenous activators (BMAL1/CLOCK/BMAL1-CLOCK/dCLOCK) have longer half-life than the endogenous repressors (PER/PER^P/CRY/dPER) in mice fibroblasts and *Drosophila* S2 cells. This implies that feedback loops for the activators are slower than those of the repressors in the circadian clocks because the degradation rates of the components of the feedback loops are the key step that determines the time scale of a feedback loop. These data come from the following experimental studies: PER: Unphosphorylated PER1, 2 (Lee et al, 2009), PER^P: Phosphorylated PER1, 2 (Meng et al, 2008), CRY: CRY1, 2 (Chen et al, 2009; Meng et al, 2008; Siepka et al, 2007), BMAL1: CLOCK unbinding BMAL1 (Kwon et al, 2006), CLOCK: BMAL1 unbinding (Kwon et al, 2006) CLOCK (Kwon et al, 2006), BMAL1-CLOCK: dimer BMAL1-CLOCK (Kwon et al, 2006), dPER: PER in *Drosophila* S2 cells (Syed et al, 2011), and dCLOCK: CLOCK in *Drosophila* S2 cells (Lamaze et al, 2011).

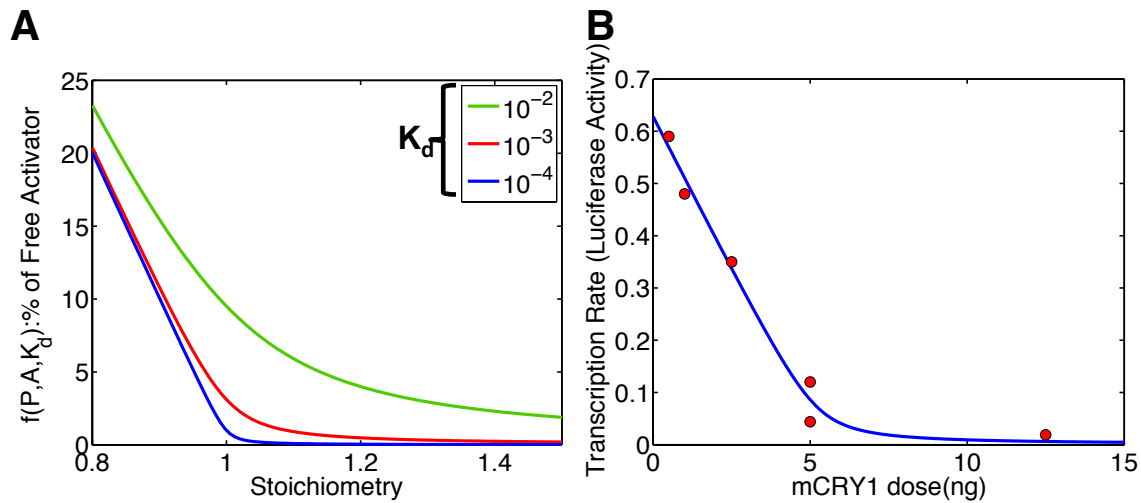
7. Supplementary Figures



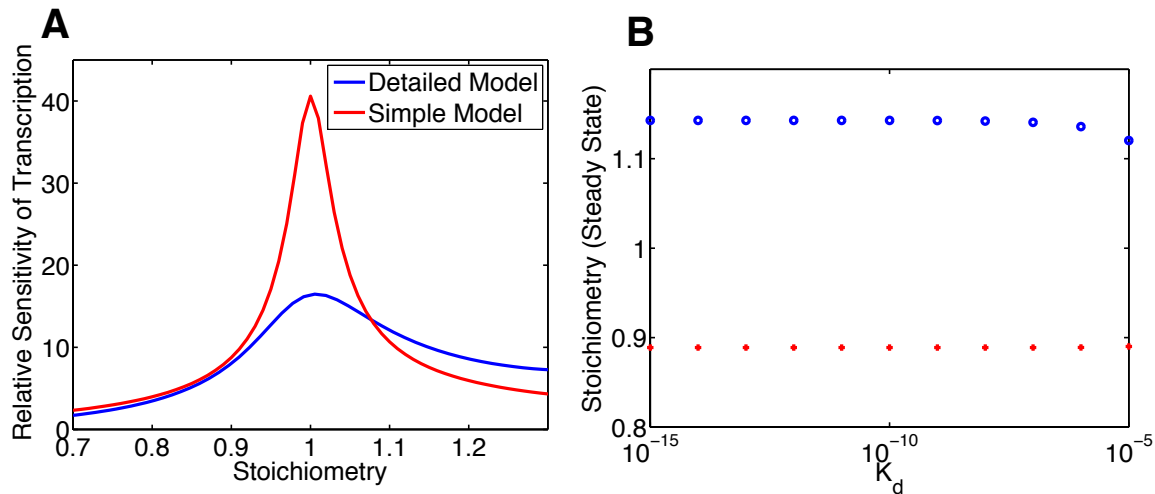
Supplementary Figure 1. Top 10 ranked sensitivities for period. The changes of period are measured in the presence of 1% perturbation of each parameter. Relative sensitivity equation used is

$$\text{Relative Sensitivity} = \frac{d(\text{Period})}{d(\text{Parameter})} \frac{\text{Parameter}}{\text{Period}} = \frac{d \ln(\text{Period})}{d \ln(\text{Parameter})}$$

The model shows large sensitivities to perturbation of parameters related with degradation rate or phosphorylation of PER2.



Supplementary Figure 2. The transcription rate control by protein sequestration of the simple model matches experimental data. **(A)** The fraction of the free activator, $f(P, A, K_d)$, with various dissociation constants, K_d . As dissociation constant between the activator (A) and the repressor (P) decreases, the fraction of free activator decreases or transcription rate decreases. Here, $A=0.0659$. **(B)** The effects of mCRY1 expression on CLOCK:BMAL1 activated transcription. Data are taken from Figure 2 and Supplementary Figure 2 of (Froy et al, 2002). Our model can easily match this data.

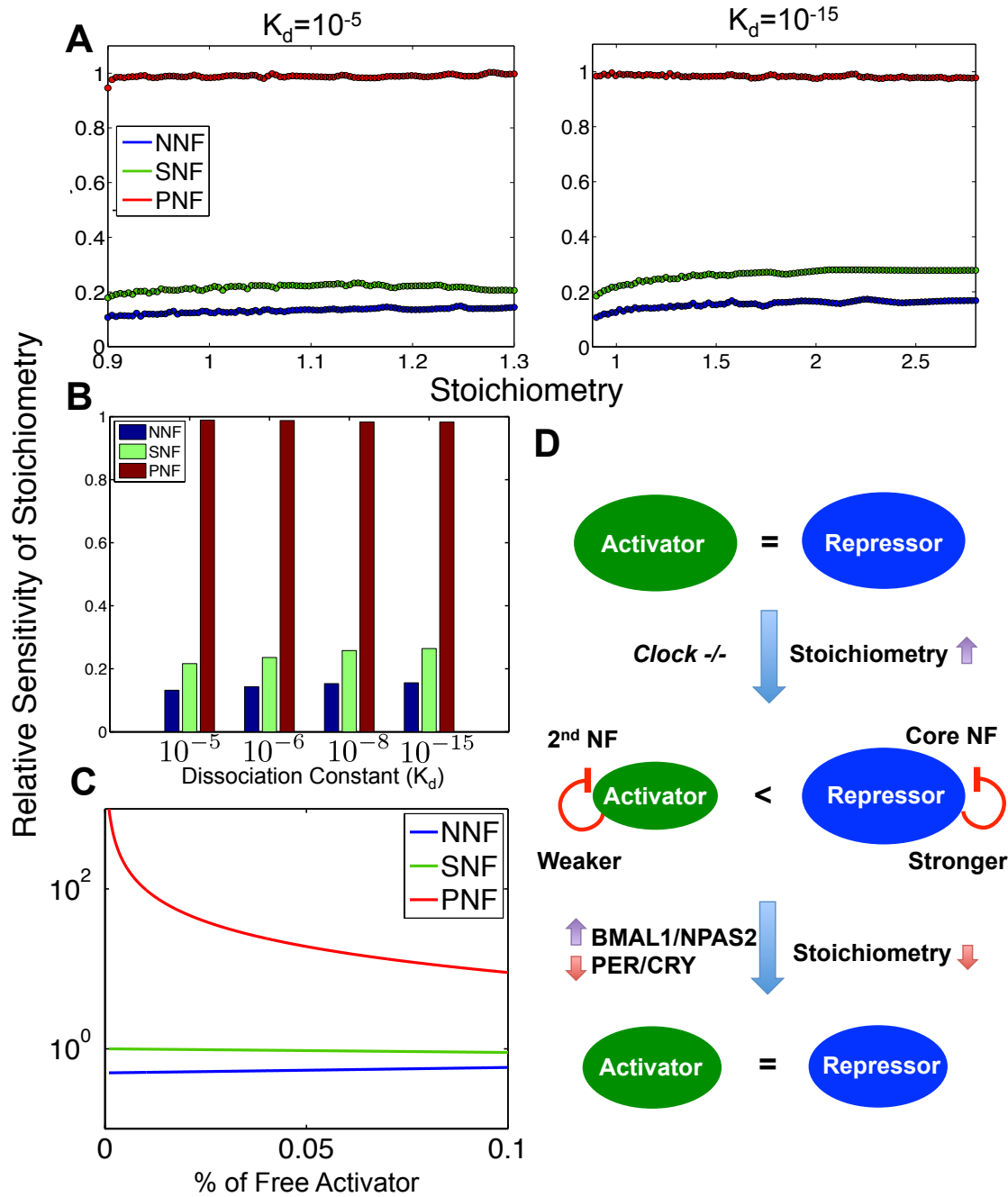


Supplementary Figure 3. 1-1 stoichiometry generates an ultrasensitive response. (A)

The relative sensitivity of transcription rate of repressors is the highest at 1-1 stoichiometry in both the detailed and the simple model. From the solutions of model, we calculated

$$\text{Relative Sensitivity} = \frac{d(\% \text{ of Free Activators})}{d(\text{Stoichiometry})} \frac{\text{Stoichiometry}}{\% \text{ of Free Activators}}$$

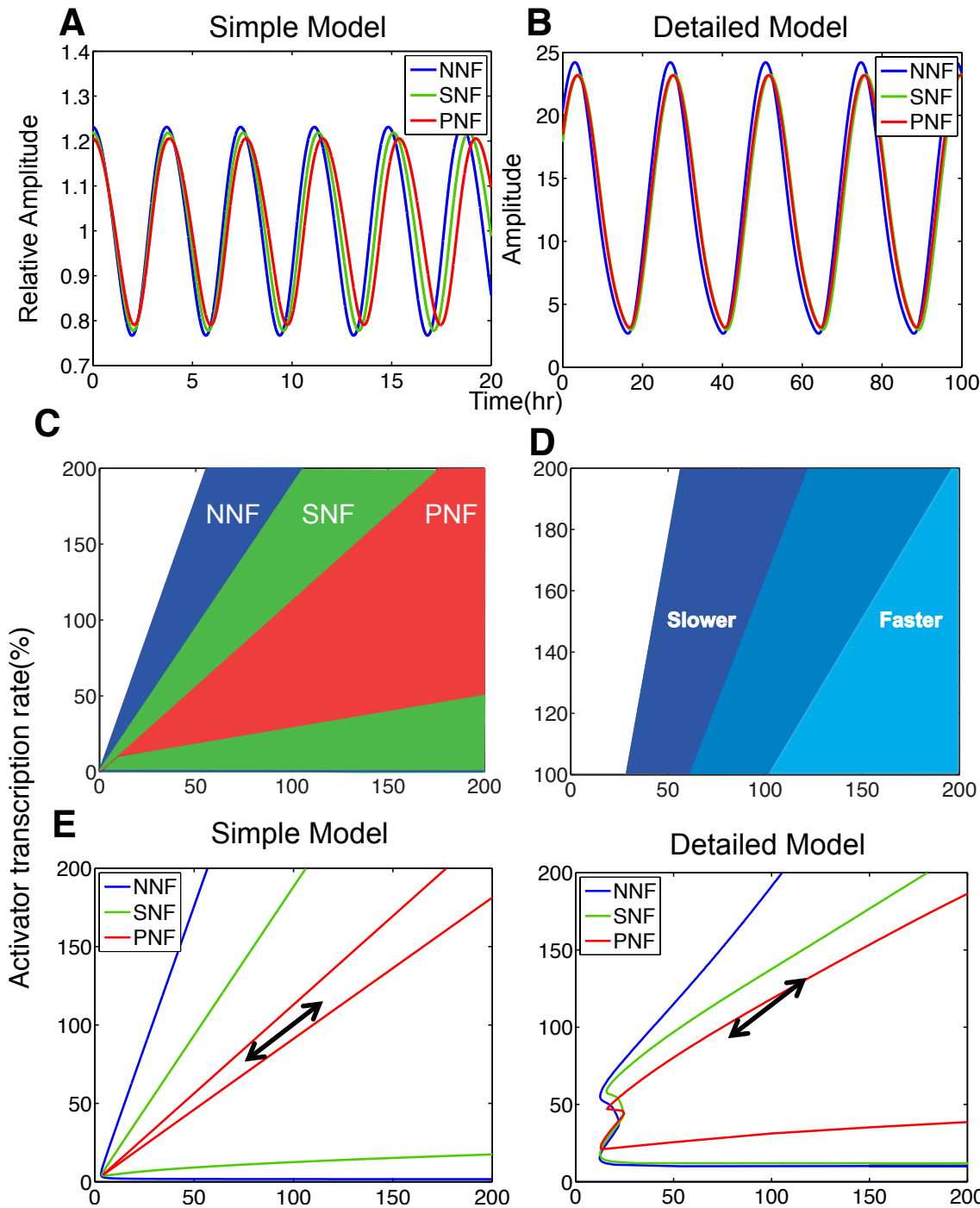
(See Supplementary Figures 4A for the parameters used). **(B)** The upper and lower bound of steady state of stoichiometry where the simple model oscillates. See “Analysis showing that a balanced stoichiometry promotes oscillations” in the Supplementary information for details.



Supplementary Figure 4. Controlling the activator concentration with an additional negative feedback loop maintains stoichiometry in balance. (A) The relative sensitivity of the stoichiometry with respect to transcription rate change in the SNF, NNF, and PNF was measured over the range of transcription rates with which the stoichiometry are in the appropriate range for rhythm generation seen Figure 3D. The relative sensitivity equation used is

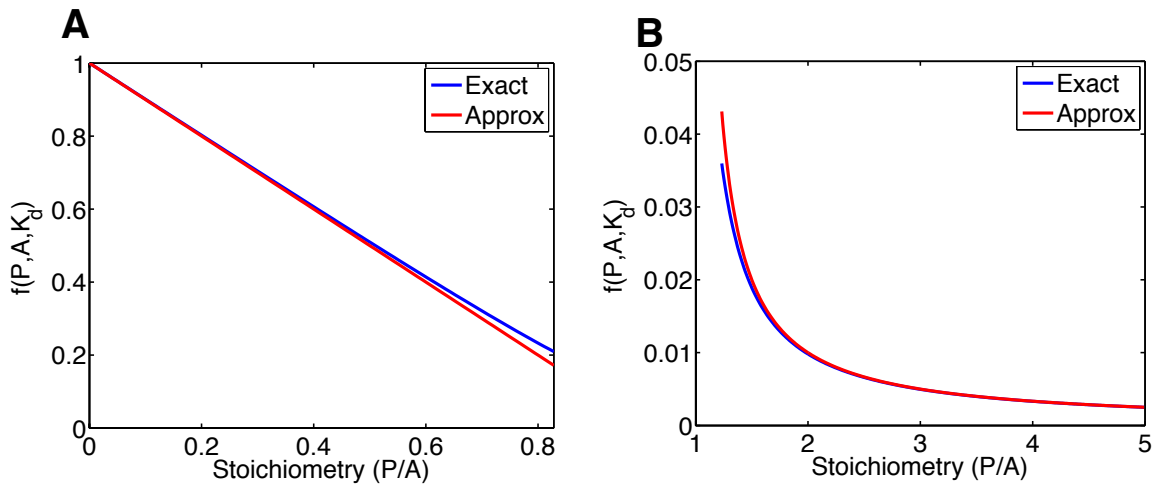
$$\text{Relative Sensitivity} = \frac{d(\text{Stoichiometry})}{d(\text{Transcription Rate})} \frac{\text{Transcription Rate}}{\text{Stoichiometry}}$$

This equation is the % change in the stoichiometry (repressor/activator) per % change in transcription rate of repressor. **(B)** We calculated the average of relative sensitivity over the range of parameters. On average, the relative sensitivity of the NNF model is about 2 fold less sensitive than that of the SNF model, but that of the PNF model is about 4 fold more sensitive than that of the SNF model regardless of the binding affinity. This implies that the NNF is best to maintain the stoichiometry balance when the transcription rate is perturbed. (Here we assumed $\delta=0.2$. When this assumption was relaxed, the result is similar. See Supplementary information and Supplementary Figure 4C). **(C)** Relative sensitivity of the steady state of % of free activator for the general parameters of the simple models with different structures (see “Analysis of the role of an additional feedback loop in balancing stoichiometry” in Supplementary information for the details). **(D)** The schematic explanation how the NNF structure maintains the stoichiometric balance. *Clock-* increases the stoichiometry (repressors/activators) because the activator decreases. The increased stoichiometry strengthens the core negative feedback and reduces the expression of the repressors and Rev-erbs. This weakens the additional negative feedback loop and increases the expression of other activators. The reduced expression of the repressors and increased expression of the activators decrease the increased stoichiometry to 1-1.



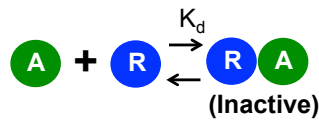
Supplementary Figure 5. The NNF structure oscillates over the widest range of parameters. (A-B) To compare the robustness of the three feedback loop structures (NNF, SNF and PNF), parameters for the activators were selected to make the timecourses of the repressors in the three structures similar. (A) The repressor (P) time profiles of simple models of the three structures. The amplitude is normalized by its

average value. Here, we assumed $K_d = 10^{-5}$ and $\delta = 0.2$. γ in the NNF model and the PNF model were selected as 0.0043 and 0.0395, which made the NNF model and the PNF model have the same average activator concentration as in the SNF model ($A=0.0659$). With these parameters models have a similar stoichiometry, amplitude and period. **(B)** The Per2 mRNA time profile of detailed mammalian circadian clock models with three types of structures. In the SNF model, the level of the oscillating activators (Bmals and Npas2) is fixed at the average level in the original model (NNF). Transcription of Bmals and Npas2 are activated with E-box activation in the PNF model while they are repressed with E-box activation through REV-ERBs in the original model (NNF). **(C)** The NNF structure has the widest range of parameters where the model oscillates regardless the dissociation constant. Here, K_d is decreased to 10^{-15} from 10^{-5} in Figure 5A. The range of parameters where the system oscillates is shown when the transcription rate of the repressor and activator were changed from their initial value (100%). As the dissociation constant decreases, the ranges of parameters, where the system oscillates, increase in all three structures. Here we assumed $\delta=0.2$ **(D)** A slower additional feedback loop (i.e. more stable activator) increases the range of parameters for which the system oscillates in NNF. Here, δ is changed from 0.2 to 3. γ is also changed from 0.0043 to 0.0645 to keep the same expression levels of the activator. Other parameters are the same with those in Figure 5A. **(E)** For a significant increase or decrease of transcription rate of both activator and repressor, both the simple model and the detailed model still show sustained oscillations. All structures (NNF, SNF and PNF) oscillate when transcription rate of both repressor and activator increases or decreases by the same amount because the stoichiometry is still balanced for the change. The PNF, SNF and NNF models oscillate inside of red, green and blue line, respectively. The bifurcation lines, which indicate where oscillations in the system are lost, were calculated with XPP-AUTO.



Supplementary Figure 6. Approximation of free activator functions in the simple model. **(A)** Approximation of $f(P, A, K_d)$ with $1 - P / A$ when $P / A < 1 - (2\sqrt{2\varepsilon^2 + 3\varepsilon} - 2\varepsilon)$ and $\varepsilon = K_d / A$ is small. Here, $A = 10^{-3}$ and $K_d = 10^{-5}$. See “Analysis showing that a balanced stoichiometry promotes oscillations” in Supplementary information for details. **(B)** Approximation of $f(P, A, K_d)$ with $\varepsilon / (P / A - 1)$ when $P / A > 1 + (2\sqrt{2\varepsilon^2 + \varepsilon} + 3\varepsilon)$.

Sequestration (New Model)



Modeling
Math Analysis

Tight binding increases the robustness of rhythms (Figure 3)

Tight binding is necessary for rhythm generation (Sato et al (2006))

Transcription rates for repressor concentration indicates tight binding (Froy et al (2002))

1-1 Stoichiometry is necessary to generate the rhythms (Figure 3)

1-1 Stoichiometry in transcription regulation (Menet et al (2009))

In vivo evidence for role of 1-1 stoichiometry (Lee et al (2011))

Resilience to change in overall transcription rate (Dibner et al (2009))

1-1 stoichiometry generates ultra-sensitivity (Buchler et al (2009))

Stoichiometry is much less than 1-1 in *Neurospora* clock (He et al (2005))

2nd Negative feedback loop increase the robustness of rhythms and period (Figures 4 - 6)

Gene does analysis implies that the clock balances the stoichiometry through NNF (Baggs et al (2009))

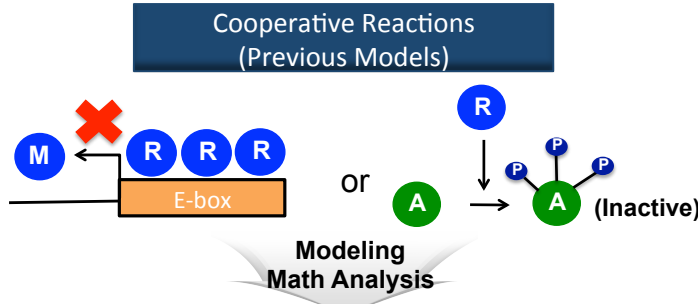
2nd Negative feedback loop play more dominant role than 2nd positive feedback loop (Liu et al (2008))

Loss of part of 2nd negative feedback loop increase the deviation of period (Preitner et al (2001))

The half-life of activators are significantly longer than the half-life of repressors (Table S4)

2nd negative feedback loop has not been identified in *Neurospora* clock (Baker et al (2012)).

Supplementary Figure 7. Comparison of the predictions of the new model and experimental data. The predictions of the new model based on the protein sequestration match experimental data of circadian clocks of higher organisms, but not *Neurospora* circadian clocks.



High Hill-coefficient is important to generate the rhythms

Co-operative reactions through multiple e-boxes binding may not be required (Yoo et al (2005))

Multiple-phosphorylation sites of WCC are required for rhythms in *Neurospora* Clock (Huang et al (2007))

2nd Negative feedback loop does not play any role

Loss of 2nd negative feedback loop disrupts the circadian rhythms (Cho et al (2012))

Loss of 2nd negative feedback loop disrupts the rhythms of activators (Liu et al (2008))

2nd negative feedback loop has not been identified in *Neurospora* clock (Baker et al (2012))

2nd Negative feedback loop maintains the rhythms when core feedback loop does not work

Loss of core negative feedback function disrupts the rhythms of activators controlled by 2nd negative feedback loop (Sato et al (2006))

Supplementary Figure 8. Comparison of the predictions of the previous models and experimental data. The predictions of the previous models based on the cooperative reactions (e.g. cooperative binding or phosphorylation on multiple sites) match experimental data of *Neurospora* circadian clocks, but not higher organisms circadian clocks (Becker-Weimann et al, 2004; Griffith, 1968; Leloup & Goldbeter, 2004; Relógio et al, 2011).

9. Equations of the detailed model

Promoter Activity

E-box

$$GR' = bin^*(Sum[x[0][kk][0][1][1], {kk, 1, 2}])^*(1-G-GR)-unbin^*GR$$

$$G' = bin^*x[0][0][1][1]^*(1-G-GR)-unbin^*G$$

$$GrR' = binr^*(Sum[x[0][kk][0][1][1], {kk, 1, 2}])^*(1-Gr-GrR)-unbinr^*GrR$$

$$Gr' = binr^*x[0][0][1][1]^*(1-Gr-GrR)-unbinr^*Gr$$

$$GcR' = binc^*(Sum[x[0][kk][0][1][1], {kk, 1, 2}])^*(1-Gc-GcR)-unbinc^*GcR$$

$$Gc' = binc^*x[0][0][1][1]^*(1-Gc-GcR)-unbinc^*Gc$$

RORE

$$GBR' = binrev^*(revn+revng+revngp+revnp)*GB-unbinrev^*GBR$$

$$GB' = -binrev^*(revn+revng+revngp+revnp)*GB+unbinrev^*GBR$$

$$GBRb' = binrevb^*(revn+revng+revngp+revnp)*GBb-unbinrevb^*GBRb$$

$$GBb' = -binrevb^*(revn+revng+revngp+revnp)*GBb+unbinrevb^*GBRb$$

Transcription

$$MnPo' = trPo^*G-tmc^*MnPo-umPo^*MnPo$$

$$McPo' = tmc^*MnPo-umPo^*McPo$$

$$MnPt' = trPt^*G-tmc^*MnPt-umPt^*MnPt$$

$$McPt' = tmc^*MnPt-umPt^*McPt$$

$$MnRt' = trRt^*Gc-tmc^*MnRt-umRt^*MnRt$$

$$McRt' = tmc^*MnRt-umRt^*McRt$$

$MnRev' = trRev^*x[0][0][0][1][1]^*Gr-tmcrev^*MnRev - umRev^*MnRev$
 $McRev' = tmcrev^*MnRev - umRev^*McRev$
 $MnRo' = trRo^*G^*GB-tmc^*MnRo - umRo^*MnRo$
 $McRo' = tmc^*MnRo - umRo^*McRo$
 $MnB' = trB^*GBb-tmc^*MnB - umB^*MnB$
 $McB' = tmc^*MnB - umB^*McB$
 $MnNp' = trNp^*GB - tmc^*MnNp - umNp^*MnNp$
 $McNp' = tmc^*MnNp - umNp^*McNp$

Secondary Loop

$B' = tlB^*McB - cbIn^*B^*Cl + uncbin^*BC - ub^*B$
 $Cl' = tlNp^*McNp + tlC - cbIn^*B^*Cl + uncbin^*BC - uc^*Cl$
 $BC' = cbIn^*B^*Cl - uncbin^*BC - phos^*BC - ubc^*BC$
 $cyrev' = tlrev^*McRev - (nlrev + urev)^*cyrev - ag^*cyrev^*(x[0][0][2][0][0]) + nerev^*revn + dg^*cyrevg$
 $revn' = -(nerev + urev)^*revn - ag^*Nf^*revn^*(x[0][0][2][1][0]) + nlrev^*cyrev + dg^*(revng)$
 $cyrevg' = ag^*cyrev^*x[0][0][2][0][0] - (dg + gto + urev + nlrev)^*cyrevg + nerev^*revng$
 $revng' = ag^*Nf^*revn^*x[0][0][2][1][0] - (dg + gto + urev + nerev)^*revng + nlrev^*cyrevg$
 $cyrevgp' = gto^*cyrevg - (dg + uprev + nlrev)^*cyrevgp + nerev^*revngp$
 $revngp' = gto^*revng - (dg + uprev + nerev)^*revngp + nlrev^*cyrevgp$
 $cyrevp' = dg^*(cyrevgp) - (uprev + nlrev)^*cyrevp + nerev^*revnp$
 $revnp' = dg^*(revngp) - (uprev + nerev)^*revnp + nlrev^*cyrevp$

Translation

$x[j][k][l][m][n]' =$

```

If[(j=1)&&(k=0)&&(l=0)&&(m=0)&&(n=0),tlp*McPo,0]
+If[(j=3)&&(k=0)&&(l=0)&&(m=0)&&(n=0),tlp*McPt,0]
+If[(j=0)&&(k=1)&&(l=0)&&(m=0)&&(n=0),tlr*McRo,0]
+If[(j=0)&&(k=2)&&(l=0)&&(m=0)&&(n=0),tlr*McRt,0]

```

Binding/Unbinding

PER-CRY

```

x[j][k][l][m][n]'=
If[(k=0)&&(n=0)&&((j=2)|||j=4)|||j=5)|||j=6),-
ar*If[m=1,Nf,1]*Sum[x[0][kk][0][m][0],{kk,1,2}]*x[j][k][l][m][n]+dr*Sum[x[j][kk][l][m][n],{kk,1,
2}],0]+
If[(j=0)&&((k=1)|||k=2))&&(l=0)&&(n=0),-
ar*If[m=1,Nf,1]*x[j][k][l][m][n]*Sum[x[jj][0][ll][m][0],{jj,{2,4,5,6},{ll,0,3}}]+dr*Sum[x[jj][k][l][m]
[n],{jj,{2,4,5,6},{ll,0,3}}],0]+
If[((j=2)|||j=4)|||j=5)|||j=6))&&((k=1)|||k=2))&&(n=0),ar*If[m=1,Nf,1]*x[0][k][0][m][n]*x[j][0][l][
m][0]-dr*x[j][k][l][m][n],0]+
If[(k=0)&&(n=1)&&((j=2)|||j=4)|||j=5)|||j=6))&&(m=1),-
ar*Nf*x[j][k][l][m][n]*Sum[x[0][kk][0][m][0],{kk,1,2}]+dr*Sum[x[j][kk][l][m][n],{kk,1,2}],0]+
If[(j=0)&&((k=1)|||k=2))&&(l=0)&&(m=1)&&(n=0),-
ar*Nf*x[j][k][l][m][n]*Sum[x[jj][0][ll][m][1],{jj,{2,4,5,6},{ll,0,3}}]+dr*Sum[x[jj][k][l][m][1],{jj,{2,4
,5,6},{ll,0,3}}],0]+
If[((j=2)|||j=4)|||j=5)|||j=6))&&((k=1)|||k=2))&&(m=1)&&(n=1),ar*Nf*x[j][0][l][m][n]*x[0][k][0][
m][0]-dr*x[j][k][l][m][n],0]+
If[(k=0)&&(n=0)&&((j=2)|||j=4)|||j=5)|||j=6))&&(m=1),-
ar*Nf*x[j][k][l][m][n]*Sum[x[0][kk][0][m][1],{kk,1,2}]+dr*Sum[x[j][kk][l][m][1],{kk,1,2}],0]+

```

```

If[(j=0)&&((k=1)||k=2))&&(l=0)&&(m=1)&&(n=1),-
ar*Nf*x[j][k][l][m][n]*Sum[x[jj][0][ll][m][0],{jj,{2,4,5,6}},{ll,0,3}]+dr*Sum[x[jj][k][ll][m][n],{jj,{2,4
,5,6}},{ll,0,3}],0]+

If((j=2)||j=4||j=5||j=6))&&((k=1)||k=2))&&(m=1)&&(n=1),ar*Nf*x[j][0][l][m][0]*x[0][k][0][
m][1]-dr*x[j][k][l][m][n],0]+

If[(l=0)&&(j>0)&&(n=0),ac*If[m=1,Nf,1]*x[j][k][l][m][n]*x[0][0][1][m][0]+dc*x[j][k][1][m][n],0]

```

PER-CKI

```

x[j][k][l][m][n]=

If[(j=0)&&(k=0)&&(l=1)&&(n=0),-
ac*If[m=1,Nf,1]*x[j][k][l][m][n]*Sum[x[jj][kk][0][m][0],{jj,1,6},{kk,0,2}]+dc*Sum[x[jj][kk][l][m][
0],{jj,1,6},{kk,0,2}],0]+

If[(j>0)&&(l=1)&&(n=0),ac*If[m=1,Nf,1]*x[0][0][1][m][0]*x[j][k][0][m][n]-dc*x[j][k][l][m][n],0]+

If[(l=0)&&(j>0)&&(m=1)&&(n=1),-
ac*Nf*x[j][k][l][m][n]*x[0][0][1][m][0]+dc*x[j][k][1][m][n],0]+

If[(j=0)&&(k=0)&&(l=1)&&(m=1)&&(n=0),-
ac*Nf*x[j][k][l][m][n]*Sum[x[jj][kk][0][m][1],{jj,1,6},{kk,0,2}]+dc*Sum[x[jj][kk][l][m][1],{jj,1,6},{kk,0,2}],0]+

If[(j>0)&&(l=1)&&(m=1)&&(n=1),ac*Nf*x[0][0][1][m][0]*x[j][k][0][m][n]-dc*x[j][k][l][m][n],0]+

If[(j>2)&&(l=2)&&(n=0),-
ac*If[m=1,Nf,1]*x[j][k][l][m][n]*x[0][0][1][m][0]+dc*x[j][k][3][m][n],0]+

If[(j=0)&&(k=0)&&(l=1)&&(n=0),-
ac*If[m=1,Nf,1]*x[j][k][l][m][n]*Sum[x[jj][kk][2][m][0],{jj,3,6},{kk,0,2}]+dc*Sum[x[jj][kk][3][m][
0],{jj,3,6},{kk,0,2}],0]+

If[(j>2)&&(l=3)&&(n=0),ac*If[m=1,Nf,1]*x[0][0][1][m][0]*x[j][k][2][m][n]-dc*x[j][k][l][m][n],0]+

If[(j>2)&&(l=2)&&(m=1)&&(n=1),-
ac*Nf*x[j][k][l][m][n]*x[0][0][1][m][0]+dc*x[j][k][3][m][n],0]+

```

```

If[(j=0)&&(k=0)&&(l=1)&&(m=1)&&(n=0),-
ac*Nf*x[j][k][l][m][n]*Sum[x[jj][kk][2][m][1],{jj,3,6},{kk,0,2}]+dc*Sum[x[jj][kk][3][m][1],{jj,3,6},
{kk,0,2}],0]+
If[(j>2)&&(l=3)&&(m=1)&&(n=1),ac*Nf*x[0][0][1][m][0]*x[j][k][2][m][n]-dc*x[j][k][l][m][n],0]

```

PER-GSK3 β

```

x[j][k][l][m][n]'=
If[(j>2)&&((l=0)||l=1)),-
If[m=1,Nf,1]*agp*x[j][k][l][m][n]*x[0][0][2][m][0]+dg*x[j][k][l+2][m][n],0]+
If[(j=0)&&(k=0)&&(l=2)&&(n=0),-
If[m=1,Nf,1]*agp*Sum[x[jj][kk][ll][m][nn],{jj,3,6},{kk,0,2},{ll,0,1},{nn,0,1}]*x[j][k][l][m][n]+dg*
Sum[x[jj][kk][ll][m][nn],{jj,3,6},{kk,0,2},{ll,2,3},{nn,0,1}],0]+
If[(j>2)&&((l=2)||l=3)),If[m=1,Nf,1]*agp*x[j][k][l-2][m][n]*x[0][0][2][m][0]-dg*x[j][k][l][m][n],0]

```

PER-BMALs-CLOCK/NPAS2

```

x[j][k][l][m][n]'=
If[(j>0)&&(m=1)&&(n=0),-bbin*Nf*x[j][k][l][m][n]*x[0][0][0][m][1]+unbbin*x[j][k][l][m][1],0]+
If[(j=0)&&(k=0)&&(l=0)&&(m=1)&&(n=1),-
bbin*Nf*Sum[x[jj][kk][ll][m][0],{jj,1,6},{kk,0,2},{ll,0,3}]*x[j][k][l][m][n]+unbbin*Sum[x[jj][kk][ll][
m][n],{jj,1,6},{kk,0,2},{ll,0,3}],0]+
If[(j>0)&&(m=1)&&(n=1),bbin*Nf*x[j][k][l][m][0]*x[0][0][0][m][n]-unbbin*x[j][k][l][m][n],0]

```

CRY-BMALs-CLOCK/NPAS2

```

x[j][k][l][m][n]'=
If[(j=0)&&(k>0)&&(l=0)&&(m=1)&&(n=0),-
cbbin*Nf*x[j][k][l][m][n]*x[0][0][0][m][1]+uncbbin*x[j][k][l][m][1],0]+

```

```

If[(j=0)&&(k=0)&&(l=0)&&(m=1)&&(n=1),-
cbbin*Nf*Sum[x[0][kk][0][m][0],{kk,1,2}]*x[j][k][l][m][n]+uncbbin*Sum[x[0][kk][0][m][n],{kk,1
,2}],0]+
If[(j=0)&&(k>0)&&(l=0)&&(m=1)&&(n=1),cbbin*Nf*x[j][k][l][m][0]*x[0][0][0][m][n]-
uncbbin*x[j][k][l][m][n],0]+

```

REV-ERBs-GSK3 β

```

x[j][k][l][m][n]=
If[(j=0)&&(k=0)&&(l=2)&&(m=0)&&(n=0),-
ag*cyrev*x[j][k][l][m][n]+(dg)*cyrevg+(dg)*cyrevgp,0]+
If[(j=0)&&(k=0)&&(l=2)&&(m=1)&&(n=0),-
ag*Nf*revn*x[j][k][l][m][n]+(dg)*revng+(dg)*revngp,0]

```

Translocation

PER binding proteins

```

x[j][k][l][m][n]=
If[((j=2)|||j=4)|||j=5)|||j=6))&&(m=1),-
ne*If[(n=0),1,0]*x[j][k][l][m][n]+If[(n=0),1,0]*nl*x[j][k][l][0][n],0]+
If[((j=2)|||j=4)|||j=5)|||j=6))&&(m=0),ne*If[(n=0),1,0]*x[j][k][l][1][n]-
If[(n=0),1,0]*nl*x[j][k][l][m][n],0]+

```

BMALs-CLOCK/NPAS2

```

x[j][k][l][m][n]=
If[(j=0)&&(k=0)&&(l=0)&&(m=1)&&(n=1, nlbc*x[j][k][l][0][n],0)+
If[(j=0)&&(k=0)&&(l=0)&&(m=0)&&(n=1),-nlbc*x[j][k][l][m][n],0]+

```

Kinase

```

x[j][k][l][m][n]'=
If[(j=0)&&(k=0)&&((l=1)||l=2))&&(m=1)&&(n=0),-Ine*x[j][k][l][m][n],0]+
If[(j=0)&&(k=0)&&((l=1)||l=2))&&(m=0)&&(n=0),Ine*x[j][k][l][1][n],0]

```

Phosphorylation

```

x[j][k][l][m][n]'=
If[((j=1))&&(l=1)&&(k=0)&&(m=0)&&(n=0),-hoo*x[j][k][l][m][n],0]+
If[((j=2))&&(l=1)&&(k=0)&&(m=0)&&(n=0),+hoo*x[1][k][l][m][n],0]+
If[((j=3)||j=5))&&((l=1)||l=3))&&(k=0),-hto*x[j][k][l][m][n],0]+
If[((j=4)||j=6))&&((l=1)||l=3))&&(k=0),hto*x[j-1][k][l][m][n],0]+
If[((j=3)||j=4))&&((l=2)||l=3)),gto*x[j][k][l][m][n],0]+If[((j=5)||j=6))&&((l=2)||l=3)),gto*x[j-2][k][l][m][n],0]+
If[(j=0)&&(k=0)&&(l=0)&&(m=0)&&(n=1),phos*BC,0]+

```

Degradation

PER and CRY

```

x[j][k][l][m][n]'=
If[(j=0)&&(k=1)&&(l=0)&&(n=0),-uro*x[j][k][l][m][n],0]+
If[(j=0)&&(k=2)&&(l=0)&&(n=0),-urt*x[j][k][l][m][n],0]+
If[(j=0)&&(k=1)&&(l=0)&&(m=1)&&(n=1),-uro*x[j][k][l][m][n],0]+
If[(j=0)&&(k=2)&&(l=0)&&(m=1)&&(n=1),-urt*x[j][k][l][m][n],0]+
If[(j=0)&&(k=0)&&(l=0)&&(m=1)&&(n=1),uro*x[j][1][l][m][n]+urt*x[j][2][l][m][n],0]+
If[((j=1)||j=3)||j=5))&&(k=0),-If[(m=0)&&(n=1),0,1]*upu*x[j][k][l][m][n],0]+

```

```

If[((j=2)|| (j=4)|| (j=6))&&(k=0),-If[(m=0)&&(n=1),0,1]*up*x[j][k][l][m][n],0]+
If[(j=0)&&(k=0)&&(l=1)&&(n=0),up*Sum[x[jj][0][ll][m][nn],{jj,2,6,2},{nn,0,1},{ll,1,3,2}]+upu*
Sum[x[jj][0][ll][m][nn],{jj,1,5,2},{nn,0,1},{ll,1,3,2}],0]+
If[(j=0)&&(k=0)&&(l=2)&&(n=0),up*Sum[x[jj][0][ll][m][nn],{jj,2,6,2},{ll,2,3},{nn,0,1}]+upu*Su
m[x[jj][0][ll][m][nn],{jj,1,5,2},{ll,2,3},{nn,0,1}],0]+
If[(j=0)&&(k=0)&&(l=0)&&(n=1)&&(m=1),up*Sum[x[jj][0][ll][m][n],{jj,2,6,2},{ll,0,3}]+upu*Su
m[x[jj][0][ll][m][n],{jj,1,5,2},{ll,0,3}],0]

```

BMALs-CLOCK/NPAS2 and REV-ERBs

```

x[j][k][l][m][n]'=
If[(j>0)&&(k=0)&&(m=1)&&(n=1),-ubc*x[j][k][l][m][n],0]+
If[(j=0)&&(k=0)&&(l=0)&&(n=1),-ubc*x[j][k][l][m][n],0]+
If[(j>0)&&(k=0)&&(m=1)&&(n=0),ubc*x[j][k][l][m][1],0]+
If[(j=0)&&(k=0)&&(l=2)&&(m=0)&&(n=0),urev*cyrevg+uprev*cyrevgp,0]+
If[(j=0)&&(k=0)&&(l=2)&&(m=1)&&(n=0),urev*revng+uprev*revngp,0]

```

Transcriptional Activity of GSK3 β

gto'=trgto*G*GB-ugto*gto

Light Activity

```

ltn'=60*lta*(1-ltn)-ltb*ltn
MnPo'=trPo*G-tmc*MnPo-umPo*MnPo+lono*19.9*lta*(1-ltn[t])*trPo
MnPt'=trPt*G-tmc*MnPt-umPt*MnPt+lont*19.9*lta*(1-ltn[t])*trPt

```

The way to understand the equations of multi-state variables

$x[j][k][l][m][n]' = \text{If}[(j=1) \& \& (k=0) \& \& (l=0) \& \& (m=0) \& \& (n=0), tlp^* \text{McPo}, 0]$ is same with $x[1][0][0][0][0] = tlp^* \text{McPo}$. This means PER1 proteins are translated from cytoplasmic Per1 mRNA (McPo) with the rate, tlp.

$x[j][k][l][m][n]' = \text{If}[(j=0) \& \& (k=0) \& \& (l=0) \& \& (m=1) \& \& (n=1), nlbc * x[j][k][l][0][n], 0]$ is same with $x[0][0][0][1][1] = nlbc * x[0][0][0][0][1]$. This means that BMALs-CLOCK/NPAS in cytoplasm ($x[0][0][0][0][1]$) enters the nucleus and becomes $x[0][0][0][1][1]$, with rate nlbc.